Acta Pharmaceutica Sinica B 2025;15(10):5212−5230

Chinese Pharmaceutical Association
Institute of Materia Medica, Chinese Academy of Medical Sciences

Acta Pharmaceutica Sinica B

www.elsevier.com/locate/apsb
www.sciencedirect.com

ORIGINAL ARTICLE

VIRMA-mediated SHQ1 m6A modification enhances liver regeneration through an HNRNPA2B1-dependent mechanism

Hao Chen[a,b,†], Haichuan Wang[a,†], Jiwei Huang[a,†], Guoteng Qiu[a], Zheng Zhang[a], Lin Xu[a], Xiao Ma[a], Zhen Wang[a], Xiangzheng Chen[a,*], Yong Zeng[a,*]

[a]*Division of Liver Surgery, Department of General Surgery and Laboratory of Liver Surgery, and State Key Laboratory of Biotherapy, West China Hospital, Sichuan University, Chengdu 610041, China*
[b]*Department of General Surgery (Hepatopancreatobiliary surgery), the Affiliated Hospital, Southwest Medical University, Metabolic Hepatobiliary and Pancreatic Diseases Key Laboratory of Luzhou City, Luzhou 646000, China*

Received 27 February 2025; received in revised form 21 May 2025; accepted 23 May 2025

KEY WORDS

VIRMA;
m6A;
ALPPS;
Liver regeneration;
SHQ1;
HNRNPA2B1;
MeRIP-seq;
PI3K/AKT;
mRNA stability

Abstract *N*6-Methyladenosine (m6A) modification is a crucial post-transcriptional regulatory mechanism and the most abundant and highly conserved RNA epigenetic modification in eukaryotes. Previous studies have indicated the involvement of m6A modification in various tissue regeneration processes, including liver regeneration. Vir-like m6A methyltransferase associated protein (VIRMA) is an m6A methyltransferase with robust methylation capability. However, its role in liver regeneration remains poorly understood. In this study, we generated liver-specific *Virma* knockout mice using the Cre-loxP system and investigated the biological functions of VIRMA in liver regeneration using both the Associating Liver Partition and Portal vein Ligation for Staged Hepatectomy (ALPPS) mouse model and the carbon tetrachloride (CCl_4) mouse model. The expression level of VIRMA was rapidly up-regulated after ALPPS surgery and gradually down-regulated during liver repair. *Virma* deficiency significantly impaired liver regeneration capacity and disrupted cell cycle progression. Methylated RNA immunoprecipitation sequencing (MeRIP-seq) analysis revealed that *Shq1* is an effective downstream target of VIRMA-mediated m6A modification. The upregulation of *Shq1* enhanced the proliferation ability of cells, which was attenuated by the specific AKT inhibitor ipatasertib. Supplementation of *Shq1 in vivo* alleviated the liver cell proliferation inhibition caused by *Virma* deficiency. Furthermore, the m6A-binding protein

*Corresponding authors.
E-mail addresses: zengyong@medmail.com.cn (Yong Zeng), cxz090709@163.com (Xiangzheng Chen).
[†]These authors have equal contributions to this work.
Peer review under the responsibility of Chinese Pharmaceutical Association and Institute of Materia Medica, Chinese Academy of Medical Sciences.

https://doi.org/10.1016/j.apsb.2025.07.025

heterogeneous nuclear ribonucleoprotein a2b1 (HNRNPA2B1) enhanced the mRNA stability of *Shq1*. Mechanistically, *Virma* deficiency resulted in decreased m6A modification on *Shq1* mRNA, leading to reduced binding ability of m6A-binding protein HNRNPA2B1 with *Shq1*, thereby decreasing the mRNA stability of *Shq1* and reducing its protein expression level. Downregulation of *Shq1* inhibited the PI3K/AKT pathway, thereby suppressing cell proliferation and cell cycle progression, ultimately impeding liver regeneration. In summary, our results demonstrate that VIRMA plays a critical role in promoting liver regeneration by regulating m6A modification, providing valuable insights into the epigenetic regulation during liver regeneration.

1. Introduction

The liver is one of the body's most vital metabolic organs, possessing remarkable regenerative capabilities in response to stimuli to meet the demands of normal metabolism[1,2]. Studies have indicated that following partial hepatectomy (PH), hepatocytes are the primary cell type within liver tissue to re-enter the cell cycle and initiate cell division, ultimately leading to complete reconstruction of liver structure[3,4]. Decreased liver regeneration capacity results in inadequate future liver remnant (FLR) volume, leading to post-hepatectomy liver failure, also known as "small-for-size syndrome"[5], which is a major cause of mortality in patients undergoing PH. Associating Liver Partition and Portal vein ligation for Staged hepatectomy (ALPPS), as an emerging surgical strategy that rapidly promotes liver regeneration, offers the potential for curative surgery in patients previously deemed inoperable[6]. However, the molecular mechanisms underlying liver regeneration remain poorly understood. Therefore, elucidating the processes of liver regeneration, particularly the molecular mechanisms and signaling pathways involved following ALPPS surgery, holds paramount significance for the development of innovative therapeutic strategies to enhance liver regeneration.

*N*6-Methyladenosine (m6A) modification is a crucial post-transcriptional regulatory mechanism and the most abundant and highly conserved epigenetic modification on RNA in eukaryotes[7-9]. The m6A modification is achieved by adding a methyl group to the N6 position of adenosine residues in mRNA molecules, a process dynamically regulated by three homologous factors known as "writers", "readers", and "erasers" of m6A[10]. m6A modification plays critical roles in regulating RNA stability, splicing, translation, and RNA metabolism, thereby influencing various biological processes at the macroscopic level, including tissue development, differentiation, aging, regeneration, apoptosis, and immune regulation[11]. Recent studies have demonstrated that methyltransferase 3 (Mettl3), a component of the m6A methyltransferase complex, can enhance the stability and expression of *MIS12* mRNA by increasing its m6A modification level, promoting the binding of IGF2BP2 to *MIS12* mRNA, and thereby stimulating self-renewal and tissue regeneration of human mesenchymal stem cells[12]. This indicates the involvement of m6A methylation modification in tissue regeneration processes. Furthermore, the role of m6A modification in liver regeneration is increasingly being recognized. Mutations in Mettl14 suppress liver regeneration by inhibiting hepatocyte growth factor and tumor necrosis factor-alpha in non-parenchymal cells (liver sinusoidal endothelial cells, stellate cells, and Kupffer cells)[13]. Another study found that loss of Mettl14 leads to decreased m6A modification levels in mRNA molecules involved in multiple peptide processing pathways, triggering endoplasmic reticulum stress and inhibiting liver cell proliferation[14].

The m6A methyltransferase-associated protein (Vir-like m6A methyltransferase associated protein, VIRMA), also known as KIAA1429, is an essential component of the m6A methyltransferase complex and has been reported to exert a higher impact on m6A modification efficiency compared with Mettl3 and Mettl14[15]. VIRMA appears to be a pro-proliferative gene, as its involvement in various tumors, including breast cancer, nasopharyngeal carcinoma, and intrahepatic cholangiocarcinoma, has been linked to cell phenotype modulation through m6A modification[16-19]. However, the precise role of VIRMA-mediated m6A modification in liver regeneration and its potential regulatory mechanisms remain largely unexplored.

In this study, we observed an increase in VIRMA expression during liver regeneration after ALPPS surgery, accompanied by a significant elevation in global m6A levels. Liver-specific *Virma* knockout mice exhibited significantly impaired regeneration and repair capacity following ALPPS surgery or acute liver injury induced by CCL4. Mechanistically, hepatic *Virma* knockout suppressed the m6A modification level of its downstream target, *Shq1*. The reduction in m6A modification on *Shq1* mRNA decreased its binding capacity with the "reader" protein HNRNPA2B1, thereby reducing *Shq1* mRNA stability and consequently decreasing *Shq1* expression levels. SHQ1 is a critical assembly factor for H/ACA ribonucleoproteins, crucial for ribosome biogenesis and pre-mRNA splicing[20]. Previous studies have shown that loss of SHQ1 significantly inhibits cell growth[21]. Additionally, we found that the downregulation of SHQ1 expression partially hinders liver regeneration by inhibiting the PI3K/AKT signaling pathway. These findings unveil novel biological functions of VIRMA and provide new insights for potential intervention strategies in liver regeneration.

2. Materials and methods

2.1. Animals

The animal experiments were approved by the Animal Ethics Committee of West China Hospital, Sichuan University (approval code: 20080226080; July 1, 2008). Both wild-type (WT) mice and liver-specific *Virma* knockout (*Virma*-KO) mice were C57BL/6J background. The $Virma^{loxP/loxP}$ mice carrying loxP-flanked *Virma* alleles and Albumin-Cre mice were obtained from Cyagen Biosciences (Jiangsu, China). *Virma*-KO mice were generated by mating $Virma^{loxP/loxP}$ mice with Albumin-Cre mice. Genotypes were

confirmed by PCR amplification of tail DNA. All mice were housed under specific pathogen-free conditions in the Experimental Animal Center. Experiments were performed on age- and sex-matched mice aged 8−10 weeks. For the ALPPS procedure, the protocol described by Schlegel A was followed[22]. Briefly, The ALPPS procedure consists of two steps: Step 1: Using 9-0 sutures, the portal vein branches supplying the left lateral lobe, right lobe, caudate lobe, and right middle lobe were sequentially ligated, while ensuring the hepatic arterial system remained intact to achieve 90% portal vein ligation. After ligating the portal vein system to the right middle lobe, a clear ischemic line appeared immediately. Bipolar electrocautery was used to cauterize along the ischemic line, followed by transection of 80% of the liver with surgical scissors. A routine cholecystectomy was then performed. Step 2: Forty-eight hours after the first surgery, a second laparotomy was performed to resect the ischemic liver lobes, including the caudate lobe, right lobe, and right middle lobe. For the acute liver injury model, mice were challenged with intraperitoneal injection of 10 mL/kg body weight of CCl_4 (10% CCl_4 in corn oil), as previously described in our study[23]. To overexpress *Shq1* in the mouse liver, AAV8-*Shq1* (5×10^{11} genome copies/mouse) was delivered to the liver *via* tail vein injection 4 weeks before surgery. One hour before euthanasia, mice were injected intraperitoneally with 1 mg/kg BrdU (B5002, Sigma).

2.2. *Small interfering RNA transfection, plasmid transfection, and lentiviral infection*

Small interfering RNA (siRNA) targeting *Virma*, *Shq1*, and *Hnrnpa2b1* were synthesized by Tsingke Biotechnology Co., Ltd. (Beijing, China) and transfected into cells using Genmute™ reagent (SignaGen Laboratories, MD, USA). Plasmids for *Virma*, *Shq1*, and *Shq1*-MUT were synthesized by WZ Biosciences Co., Ltd. (Shandong, China), and GenJet™ plus Reagent (SignaGen Laboratories, MD, USA) was used for plasmid transfection. *Virma* and *Shq1* were cloned into lentiviral packaging vectors synthesized by WZ Biosciences Co., Ltd. (Shandong, China). Standard procedures were performed according to the multiplicity of infection of cells to achieve stable infection, and quantitative real-time polymerase chain reaction (qRT-PCR) and Western blot were used to verify transfection efficiency.

2.3. *MeRIP-seq*

After homogenizing liver tissues into cell suspensions, total RNA was isolated and purified using TRIzol reagent (Invitrogen, Carlsbad, USA). Quantification of RNA quantity and purity for each sample was conducted using NanoDrop ND-1000 (NanoDrop, Wilmington, USA), while RNA integrity was assessed using Bioanalyzer 2100 (Agilent, USA). RNA was fragmented into 100-nucleotide-long fragments using the Magnesium RNA Fragmentation Module (NEB, Ipswich, USA). Immunoprecipitation of fragmented mRNA was performed using anti-m6A antibody (Synaptic Systems, Goettingen, Germany), with 1/10 of the fragmented mRNA retained as input. RNA-seq libraries were then prepared using the KAPA Stranded mRNA-seq Kit (Illumina, San Diego, USA). Subsequently, libraries underwent paired-end sequencing on the Illumina Hiseq 4000 platform.

2.4. *Western blot*

Liver tissues and cells were lysed in RIPA Lysis Buffer (Beyotime Biotechnology, Shanghai, China) containing the protease inhibitor cocktail (Thermo Fisher Scientific, Waltham, USA). Protein concentrations were determined with the BCA protein assay kit (P0011, Beyotime, Shanghai, China). Proteins were separated by 7.5%−15% sodium dodecyl sulfate-polyacrylamide gel electrophoresis. Samples of protein were resolved on sodium dodecyl sulfate-polyacrylamide gel electrophoresis and transferred onto PVDF membranes (ISEQ00010, Millipore, Burlington, USA). The membranes were incubated with the following primary antibodies overnight at 4 °C: anti-VIRMA (68235-1-Ig, 1:1000, Proteintech, Wuhan, China), anti-CyclinD1 (#55506T, 1:1000, Cell Signaling Technology, Danvers, USA), anti-CyclinA2 (ab181591, 1:1000, Abcam, Cambridge, UK), anti-CDK2 (#2546, 1:1000, Cell Signaling Technology, Danvers, USA), anti-CyclinB1 (#4138, 1:1000,Cell Signaling Technology, Danvers, USA), anti-CDK1 (ab32094, 1:1000, Abcam, Cambridge, UK), anti-SHQ1 (bs-17473R-Bio, 1:500, bioss, Beijing, China), anti-p-AKT(Ser473) (#4060, 1:1000, Cell Signaling Technology, Danvers, USA), anti-t-AKT (#4691s, 1:1000, Cell Signaling Technology, Danvers, USA), anti-HNRNPA2B1 (14813-1-AP, 1:1000, Proteintech, Wuhan, China), anti-β-Tubulin (AF7011, 1:1000, Affinity, Jiangsu, China), anti-RICTOR (ab70374, 1:1000, abcam, Cambridge, UK), anti-GAPDH (200306, 1:5000, Zen BioScience, Chengdu, China), Secondary antibodies were pre-labelled at room temperature for 1 h. Western blots were quantified using ImageJ software (Version 1.53m).

2.5. *qRT-PCR*

Total RNA was extracted by using Trizol reagent (Invitrogen, CA, USA). Subsequently, it was converted to complementary DNA using HiScript® III All-in-one RT SuperMix (Vazyme Biotech, Nanjing, China) following the manufacturer's instruction. Real-time quantitative PCR was performed with a ChamQ™ SYBR qPCR Master Mix (Vazyme Biotech, Nanjing, China). Samples were run in triplicates, expression values were normalized against *Gapdh* and fold changes were calculated to the control group using the $2^{-\Delta\Delta CT}$ method[24]. The primers are listed in Supporting Informaiton Table S1.

2.6. *Cell proliferation assay, colony formation assays, EdU (5-ethynyl-2′-deoxyuridine) labeling assay and apoptosis analysis*

For the cell proliferation assay, cells were seeded in 96-well plates at 3×10^3 cells per well and incubated at 37 °C for 24, 48, 72 or 96 h 10 μL of cell counting kit-8 (CCK-8) reagent (Beyotime Biotechnology, Shanghai, China) was added to each well and incubated at 37 °C for 1 h. Then, the absorbance was measured at 450 nm by the EonTM Microplate Reader (BioTek, VT, USA). For the colony formation assay, 500 cells per well were plated in 6-well plates and incubated for 14 days. Cells were fixed by 4% paraformaldehyde, followed by staining with 0.1% crystal violet. The visible colonies were analyzed using ImageJ software (Version 1.53m). For the EdU labeling assay, cells were seeded in 48-well plates at 1.5×10^4 cells per well in triplicate. Cell-Light™ Apollo 567 Stain Kit (RiboBio Biotechnology, Guangzhou, China) was used to assess cell proliferation according to the manufacturer's instructions. EdU-labelled cells were photographed using OBSERVER D1/AX10 cam HRC microscope (Zeiss, Oberkochen, Germany). For apoptosis analysis, the Annexin V detection kit (Annexin V-Alexa Fluor 647/PI Kit) was used following the manufacturer's instructions. Annexin V reagent was added to cells for 5 min in the dark. Subsequently, propidium

iodide buffer was added to the cells, and they were examined using a CytoFLEX Research Flow Cytometer (Beckman Coulter, CA, USA). Data analysis was conducted using InCyte software to distinguish between healthy and apoptotic cells (early and late apoptosis).

2.7. *Immunohistochemistry*

Paraformaldehyde solution was used to fix liver specimens for 24 h. Antigen retrieval was performed by heating slides in the microwave for 20 min in 0.01 mol/L citrate buffer, and 3% hydrogen peroxide was added for 10 min to quench peroxidase activity. Sections were treated with normal goat serum, followed by incubation overnight with anti-Ki67 antibody (ab16667, 1:200, Abcam), anti-BrdU antibody (#5292, 1:200, CST) or anti-p-H3S10 antibody (06−570, 1:200, Merck Millipore) at 4 °C. Incubated with secondary antibody for 1 h, stained with diaminobenzidine. The stained sections were quantified using ImageJ software (Version 1.53m).

2.8. *Immunofluorescence*

For immunofluorescence analysis, cultured cells were fixed with 4% formaldehyde for 20 min and then blocked with 5% bovine serum albumin containing 0.2% Triton X-100 for 1 h at room temperature. Anti-albumin antibody (ab207327, Abcam) was used as the primary antibody and incubated overnight at 4 °C, followed by immunostaining with Alexa Fluor 488 secondary antibody (Invitrogen, CA, USA). Nuclei were counterstained with DAPI. Visualization of immunofluorescence was observed using a confocal laser scanning microscope.

2.9. *Statistical analysis*

All data analyses in this study were performed using the statistical software SPSS version 23.0 and the graphing software GraphPad Prism version 9.0. To compare differences between two groups, we employed *t*-tests. For comparisons involving multiple groups, we utilized one-way analysis of variance to assess statistical significance. A two-tailed P value less than 0.05 was considered statistically significant ($^{*}P < 0.05$; $^{**}P < 0.01$; $^{***}P < 0.001$).

3. Results

3.1. *VIRMA is elevated during liver regeneration after ALPPS surgery*

To investigate the biological function of VIRMA in liver regeneration after ALPPS surgery, we constructed a mouse ALPPS model following the methods described by Schlegel et al.[22] (Fig. 1A and B). Western blot analysis showed that the expression of VIRMA exhibited a rapid increase after ALPPS surgery, reaching a peak at 48 h post-surgery, followed by a gradual decrease to levels close to baseline (Fig. 1C), suggesting a potential role of VIRMA in the early stages of liver regeneration. Given that VIRMA is a known m6A methyltransferase, we further examined the m6A modification levels in total RNA from mouse liver tissues after ALPPS surgery using spectrophotometric analysis. The results showed that, similar to the trend observed for VIRMA, the global m6A levels in liver tissues increased rapidly after ALPPS surgery, peaked at 48 h post-surgery, and then gradually declined to near-baseline levels (Fig. 1D), consistent with previous studies[14,25]. These findings suggest that VIRMA

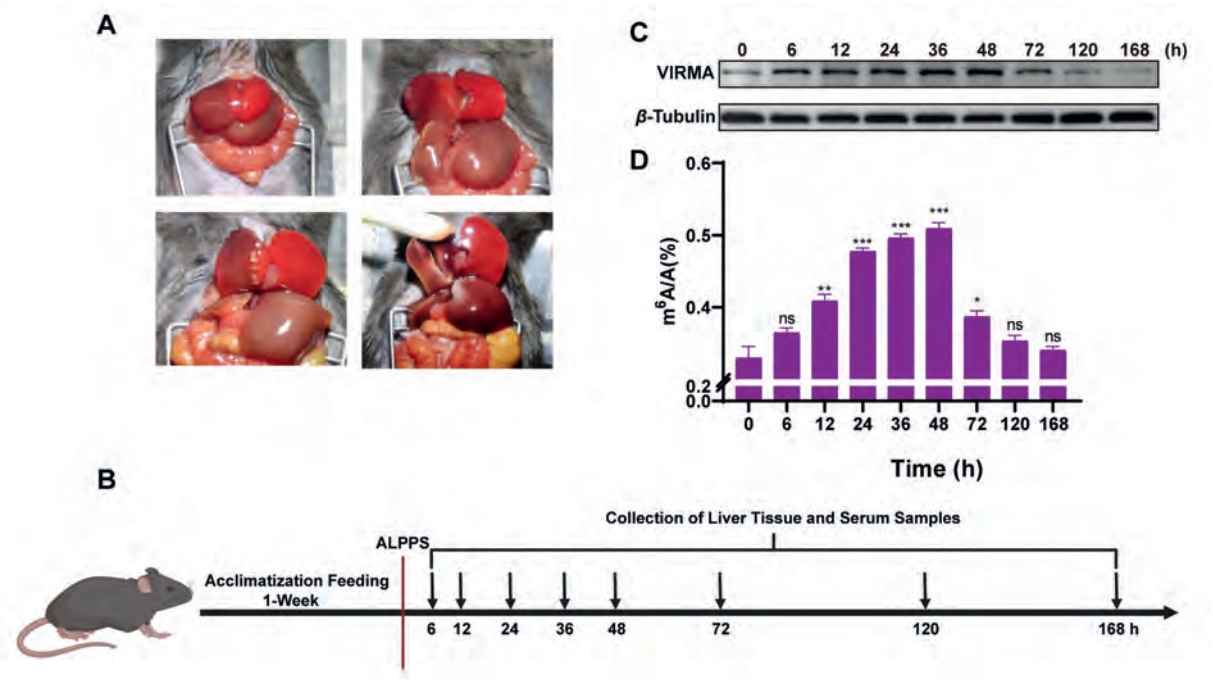

Figure 1 VIRMA and global m6A level is elevated during liver regeneration after ALPPS surgery. (A) Schematic diagram of Associating Liver Partition and Portal vein Ligation for Staged Hepatectomy (ALPPS) surgery in mice. (B) Schematic representation of the timeline for collecting liver tissue and serum samples after ALPPS surgery in mice. (C) Western blot for VIRMA expression in liver samples at specified time points after ALPPS surgery. (D) Spectrophotometric analysis of m6A modification levels in total RNA from liver tissues at designated time points post-ALPPS surgery. Data are presented as mean ± SEM ($n = 5$), $^{*}P < 0.05$; $^{**}P < 0.01$; $^{***}P < 0.001$; ns, $P > 0.05$.

may be involved in liver regeneration after ALPPS surgery, and this process may be associated with m6A modification.

3.2. *Virma knockout suppressed liver regeneration in both ALPPS and CCl_4 animal models*

To elucidate the role of *Virma* in liver regeneration, we generated liver-specific *Virma*-KO mice using the Alb-Cre/loxP system (Fig. 2A and B, Supporting Information Fig. S1A−S1C). The *Virma*-KO mice were born and grew normally, showing no abnormalities in liver size or structure based on macroscopic examination, FLR/body weight (BW), and H&E staining (Fig. S1D−S1F). Additionally, serum analyses for alanine aminotransferase (ALT), aspartate aminotransferase (AST), and total bilirubin (TBIL) levels indicated no significant changes in hepatic enzyme activity upon *Virma* deletion (Fig. S1G−S1I). We then performed ALPPS surgery on both groups of mice and assessed the degree of liver regeneration using theFLR/BW ratio. The growth rate of liver regeneration was calculated using Eq. (1):

$$\text{Growth rate} = (\text{FLR/BW at postoperative time} - \text{FLR/BW at baseline})/(\text{FLR/BW at baseline}) \quad (1)$$

As anticipated, compared with the control group, *Virma*-KO mice exhibited significantly decreased FLR/BW ratio and liver regeneration rate (Fig. 2C and D), particularly evident during the 48−72 h post-ALPPS surgery, highlighting a pronounced inhibition of liver regeneration due to *Virma* deficiency. Accordingly, *Virma*-KO mice had significantly higher serum levels of ALT, AST, and TBIL compared with the control group, suggesting that *Virma* deficiency exacerbated liver damage post-ALPPS surgery (Fig. 2E−G). Ki67 expression is indicative of cellular proliferation across all active phases of the cell cycle[26], while bromodeoxyuridine (BrdU) and phosphorylated histone H3S10 (p-H3S10) are markers of the S and G2/M phases[27]. Thus, we utilized the three markers to further evaluate hepatocellular proliferation following ALPPS surgery. The results showed the much lower Ki67-positive rates in *Virma*-KO mice compared with WT mice from 24 to 120 h post ALPPS surgery (Fig. 2H), suggesting that *Virma* deficiency may decelerate hepatocellular proliferation by inhibiting the transition from G1 to S phase. Additionally, the positive rates of BrdU and p-H3S10 were significantly lower in *Virma*-KO mouse liver tissues compared with the control group, further confirming the inhibitory effect of *Virma* deficiency on the hepatocellular cycle process. Interestingly, there is no significant differences were found in Ki67, BrdU, and p-H3S10 expression between *Virma*-KO and WT mouse liver tissues at 168 h post-ALPPS surgery, indicating a recovery of hepatocellular proliferation at the late stage of regeneration (Fig. 2I and J). Similar to these staining results, H&E staining revealed a significant reduction in mitosis (indicated by arrows) in *Virma*-KO mice compared with the control group (Supporting Information Fig. S2A). While, global m6A modification levels were found significantly lower in *Virma*-KO mice at 48 h post-ALPPS surgery compared with the WT group (Fig. 2K). Western blot analysis of cell cycle proteins revealed a significant inhibition of the key G1 phase regulator CyclinD1 expression in *Virma*-KO mouse livers during the first 72 h post-ALPPS surgery, suggesting a G1 phase arrest due to *Virma* deficiency (Fig. 2L). Moreover, the expression of S-phase-related cell cycle proteins CyclinA2 and CDK2 was significantly reduced in *Virma*-KO mice, while the expression of G2/M phase key regulators CyclinB1 and CDK1 was also significantly decreased in *Virma*-KO mouse livers (Fig. 2L), indicating the critical role of *Virma* in regulating the liver cell cycle process.

To further confirm the role of *Virma* in liver regeneration following liver injury, we utilized CCl_4 as a chemical inducer to establish an acute liver injury model, mimicking the regenerative environment post-liver damage. H&E staining results revealed that within 72 h post CCl_4 injection, both *Virma*-KO and WT mice exhibited evident hepatocellular damage, with the severity being more pronounced in *Virma*-KO mice (Fig. 3A). While WT mice had completed liver repair by 120 h post CCl_4 injection, *Virma*-KO mice still showed evidence of partial hepatic tissue necrosis at the same time point (Fig. 3A). Immunofluorescence staining for IBA1, a general macrophage marker, showed that in the WT group, the number of $IBA1^+$ cells was higher at 72 h post CCl_4 treatment compared with 48 h. A similar pattern was observed in the *Virma*-KO group. However, *Virma* knockout significantly reduced the number of $IBA1^+$ cells at both time points (Fig. S2B). Furthermore, serum biochemical analysis showed significantly higher levels of ALT, AST, and TBIL in *Virma*-KO mice compared with the control group at the same time points, suggesting a slower repair process in *Virma*-KO mice following acute liver injury (Fig. 3B−D). Western blot analysis revealed that within the first 72 h of CCl_4 treatment, the expression levels of the key regulatory protein CyclinD1 in the G1 phase was significantly inhibited in *Virma*-KO mouse liver tissues, while the expression of the S-phase markers CyclinA2 and CDK2, as well as the G2/M-phase markers CyclinB1 and CDK1, was also significantly reduced (Fig. 3E). Then, we further examined expressions of cell proliferation markers by immunohistochemical analysis, within the first 120 h after CCl_4 treatment, the positive rates of Ki67, BrdU, and p-H3S10 were significantly lower in liver tissues of *Virma*-KO mice compared with WT mice (Fig. 3F−H). To further investigate the role of *Virma* in liver regeneration, we performed PH in mice. As shown in Supporting Information Fig. S3A and S3B, the FLR/BW ratio was significantly reduced in the *Virma*-KO group compared with the control group at both 48 and 72 h post-PH (Fig. S3A). Additionally, immunohistochemical staining revealed a substantial decrease in Ki67-positive hepatocytes in the *Virma*-KO group, further confirming the impaired liver regeneration capacity following PH (Fig. S3B). These findings are consistent with those observed in the ALPPS and CCl_4 models, underscoring the critical role of *Virma* in hepatocyte proliferation and liver regeneration.

3.3. *Virma affected the proliferative capacity of AML12*

We effectively knocked down the expression levels of *Virma* in AML12 cells using siRNA (Fig. 4A, Fig. S1J). Subsequently, we assessed the proliferative capacity of AML12 cells after *Virma* knockdown through a series of biological experiments, including CCK-8 proliferation assays, colony formation assays, and EdU labeling experiments. The results consistently showed that *Virma* knockdown significantly inhibited the proliferative activity of AML12 cells (Fig. 4B−F). Furthermore, we stably overexpressed *Virma* in AML12 cells using lentivirus-mediated methods and further evaluated its proliferative capacity (Fig. 4G). Similarly, CCK-8 proliferation assays, colony formation assays, and EdU labeling experiments consistently demonstrated that *Virma* overexpression significantly enhanced the proliferative capacity of AML12 cells (Fig. 4H−L). In addition to its effect on cell proliferation, *Virma* also exerted a significant impact on the apoptotic process of AML12 cells. Flow cytometric analysis revealed that *Virma* knockdown increased the apoptosis rate of AML12 cells (Fig. S1K), while *Virma* overexpression effectively reduced the

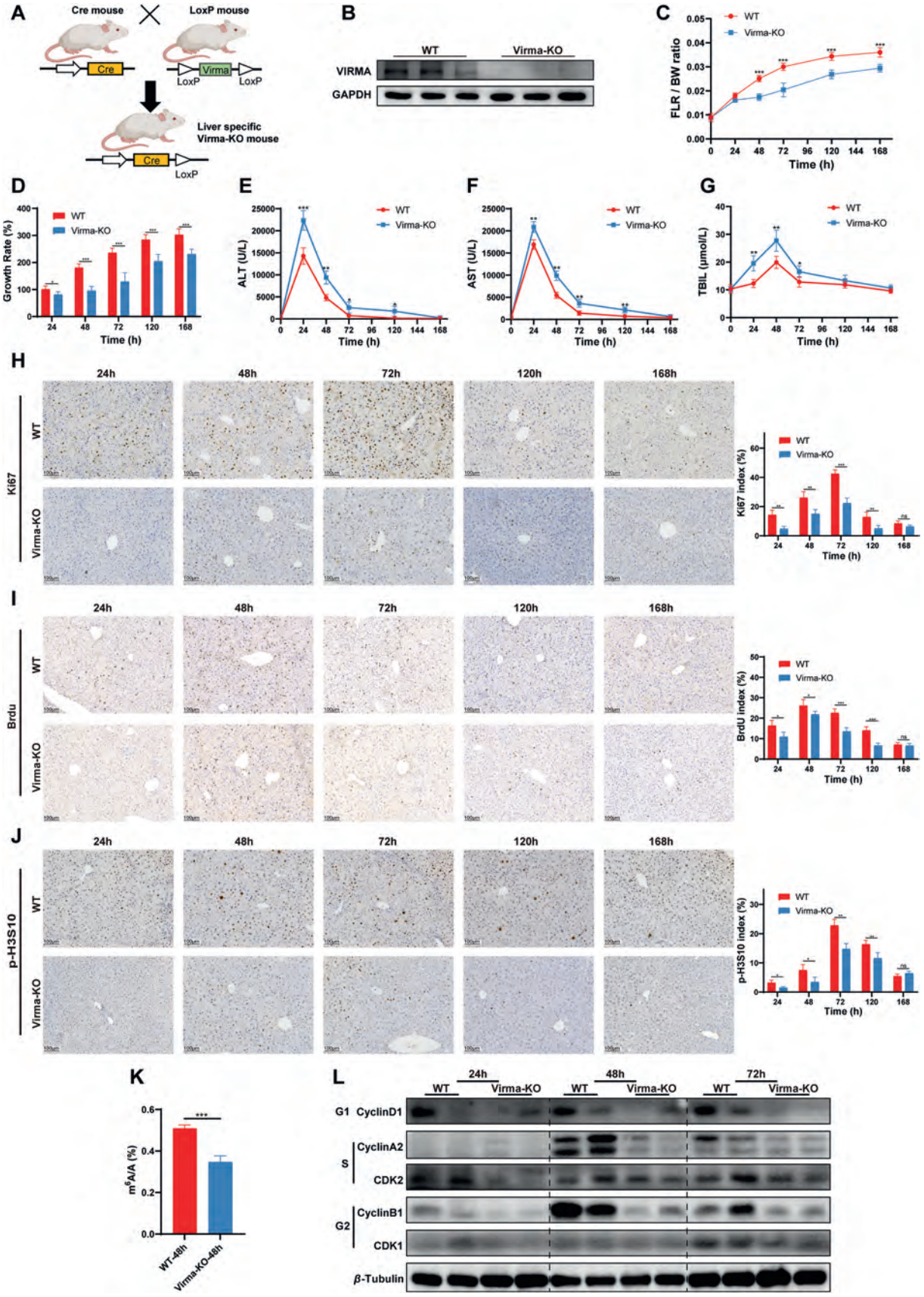

Figure 2 *Virma* knockout suppresses liver regeneration post-ALPPS surgery. (A) An overview of the strategy for the generation of liver-specific *Virma* knockout mice. (B) Western blot analysis for VIRMA expression in liver tissues of the two groups. (C) Future liver remnant (FLR)/body

apoptosis rate (Fig. S1L). These results indicate that *Virma* not only plays a crucial role in promoting the proliferation of AML12 cells but also exerts a protective effect on maintaining cell survival.

3.4. SHQ1 was identified as a downstream target of VIRMA-mediated m6A modification

Given that VIRMA is an essential component of the m6A methyltransferase complex, to further explore downstream targets of VIRMA in promoting liver regeneration, we conducted MeRIP-seq on liver tissues from WT, *Virma*-KO, WT-48 h post-ALPPS, and *Virma*-KO-48 h post-ALPPS mice. Consistent with previous reports, the canonical GGAC motif was highly enriched within m6A sites in all groups (Fig. 5A−C), and these m6A modifications were predominantly distributed in the coding sequence (CDS) and the 3′-untranslated regions[28]. Gene Ontology analysis indicated that *Virma* depletion mainly affected processes such as DNA recombination, cell cycle, and cell population proliferation during liver regeneration (Fig. 5D). Kyoto Encyclopedia of Genes and Genomes pathway analysis revealed significant enrichment of the PI3K−AKT and MAPK signaling pathways among these differentially expressed genes (Fig. 5E), both of which are known to be important pathways in liver regeneration[29,30]. Given that the global level of m6A modification increases during liver regeneration and the role of *Virma* as an m6A writer, we reasoned that the abundance of m6A would increase in the regenerating livers of WT mice but decrease in *Virma*-KO mice. Based on this, we identified 19 potential downstream target genes of *Virma* (Fig. 5F). Subsequently, we further evaluated the expression levels of these genes through qRT-PCR experiments (Supporting Information Fig. S4A−S4Q) and found that *Shq1* and *Adck2* were upregulated after ALPPS surgery and decreased after *Virma* knockout (Fig. 5G and H). Next, MeRIP-qPCR validated the increased m6A methylation levels of these two genes after ALPPS surgery and their decreased levels after *Virma* knockout (Fig. 5I and J).

To identify potential direct downstream genes of *Virma*, we conducted RIP experiments and observed a significant enrichment of *Shq1* mRNA in the products pulled down by the VIRMA antibody (Fig. 5K). However, there was no significant enrichment of *Adck2* mRNA (Fig. S4R), indicating that VIRMA interacts with *Shq1* rather than *Adck2*. Because *Shq1* has been shown to play a key role in cellular processes related to RNA processing and ribosome biogenesis[31]. VIRMA-mediated m6A modification is known to be involved in various cellular processes, including maintaining RNA stability and regulating RNA translation[32]. we hypothesized that there was a potential synergistic interaction between VIRMA and *Shq1*. To test the hypothesis, we first examined the expression levels of SHQ1 using Western blotting, which revealed a significant decrease in SHQ1 protein expression levels in *Virma*-KO mice (Fig. 5L), then, as expected, *in vitro* experiments showed that knocking down VIRMA reduced SHQ1 protein expression levels in AML12 cells, while overexpressing VIRMA increased SHQ1 levels (Fig. 5M). To further determine the mRNA stability of *Shq1*, we conducted actinomycin D experiments. Actinomycin D inhibits the synthesis of nascent mRNA and is used for mRNA stability assays[33]. We isolated primary hepatocytes from WT and *Virma*-KO mice and confirmed it with ALB immunofluorescence staining (Figs. S4S and S4T). The actinomycin D assay revealed that *Virma* knockout resulted in decreased stability of *Shq1* mRNA (Fig. 5N), while *Virma* overexpression enhanced the stability of *Shq1* mRNA (Fig. 5O). These data indicate that VIRMA acts as an upstream regulatory factor of SHQ1, whereby it regulates the expression of *SHQ1* by stabilizing its mRNA. Subsequently, we used the SRAMP database to predict m6A methylation sites on *Shq1* (Fig. 5P) and synthesized pmirGLO-*Shq1*-WT luciferase reporter genes containing the WT *Shq1* CDS region. For the control group, we followed previous research findings[34] and constructed a mutant *Shq1* encoding region in pmirGLO-*Shq1*-MUT luciferase reporter gene by replacing the adenine (A) at the m6A site with cytosine (C). Results from the dual luciferase reporter system showed that pmirGLO-*Shq1*-WT luciferase activity significantly decreased after knocking down *Virma*, while there was no statistical change in pmirGLO-*Shq1*-MUT luciferase activity after knocking down *Virma* (Fig. 5Q), indicating that the regulation of *Shq1* expression by *Virma* depends on m6A modification.

3.5. SHQ1 promotes cell proliferation through an AKT activation-dependent mechanism, while the loss of VIRMA inhibits cell proliferation by suppressing SHQ1 expression

To elucidate the biological function of SHQ1, we successfully reduced the expression level of SHQ1 in the AML12 cell line using siRNA (Fig. 6A and B). Through assessments of proliferation capacity using CCK-8 assays, colony formation experiments, and EdU labeling assays, we found that the downregulation of SHQ1 significantly attenuated the proliferation ability of AML12 cells (Fig. 6C−G). Consistent with these findings, *in vivo* experiments revealed that *Shq1* knockdown markedly reduced the number of $Ki67^+$ proliferating cells (Supporting Information Fig. S5A) and led to a significant increase in serum ALT (Fig. S5B) and AST levels (Fig. S5C), indicative of impaired liver regeneration and sustained liver injury. Consistently, *Shq1* overexpression significantly increased the FLR/BW ratio at 48 and 72 h post-ALPPS (Fig. S5D). Moreover, the number of $Ki67^+$ proliferating cells in the liver was markedly elevated in *Shq1*-overexpressing mice compared with controls (Fig. S5E). These results suggest that *Shq1* plays a critical role in hepatocyte proliferation and liver regeneration. To determine whether the regulatory effect of VIRMA is mediated by SHQ1, we conducted rescue experiments and found that the overexpression of VIRMA

weight (BW) ratios of the two groups mice at specified time points post-Associating Liver Partition and Portal vein Ligation for Staged Hepatectomy (ALPPS) surgery. (D) Liver regeneration rates of the two groups mice at specified time points post-ALPPS surgery, calculated by the formula: (FLR/BW at postoperative time−FLR/BW at baseline)/(FLR/BW at baseline). (E−G) Levels of ALT, AST, and TBIL in serum samples of mice at specified time points post-ALPPS surgery. (H−J) Immunohistochemical staining results for Ki67, BrdU, and p-H3S10 in liver tissues of the two groups mice at specified time points post-ALPPS surgery, along with statistical analysis of the percentage of positive cells (scale bar = 100 μm). (K) Spectrophotometric analysis of m6A modification levels in total RNA extracted from liver tissues of the two groups mice at 48 h post-ALPPS surgery. (L) Western blot analysis for CyclinD1, CyclinA2, CDK2, CyclinB1, and CDK1 in liver tissues of the two groups mice at 24, 48, and 72 h post-ALPPS surgery. G1 phase protein: CyclinD1; S phase proteins: CyclinA2 and CDK2; G2 phase proteins: CyclinB1 and CDK1. Data are presented as mean ± SEM ($n = 5$), $^*P < 0.05$; $^{**}P < 0.01$; $^{***}P < 0.001$; ns, $P > 0.05$.

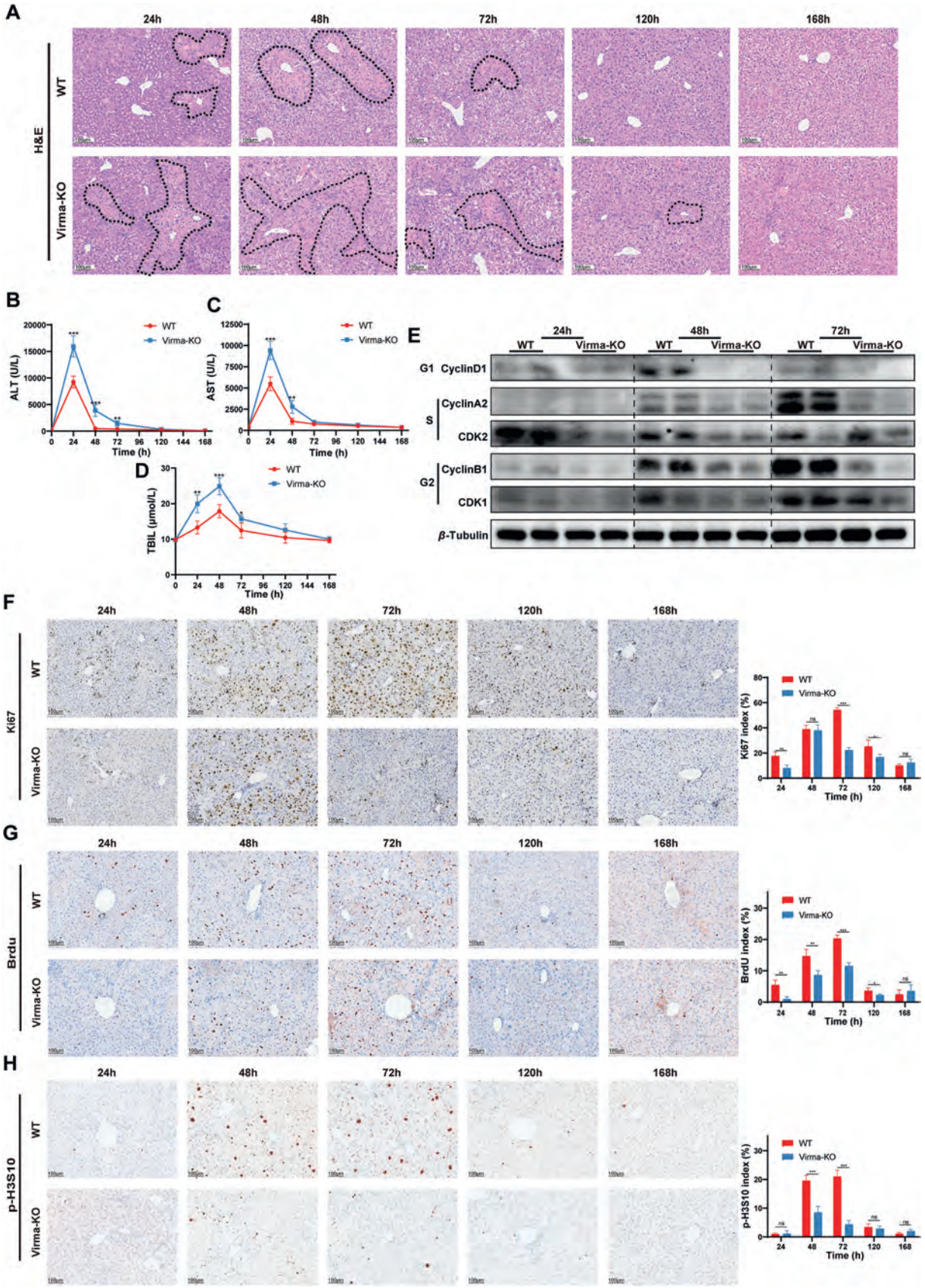

Figure 3 *Virma* deficiency impairs liver repair after CCl_4 challenge. (A) H&E staining depicting the extent of hepatic necrotic areas at specified time points following carbon tetrachloride (CCl_4) treatment in two groups. (B−D) Serum levels of ALT, AST, and TBIL in mice at specified time points post CCl_4 treatment. (E) Western blot analysis for CyclinD1, CyclinA2, CDK2, CyclinB1, and CDK1 in liver tissues of two groups at 24,

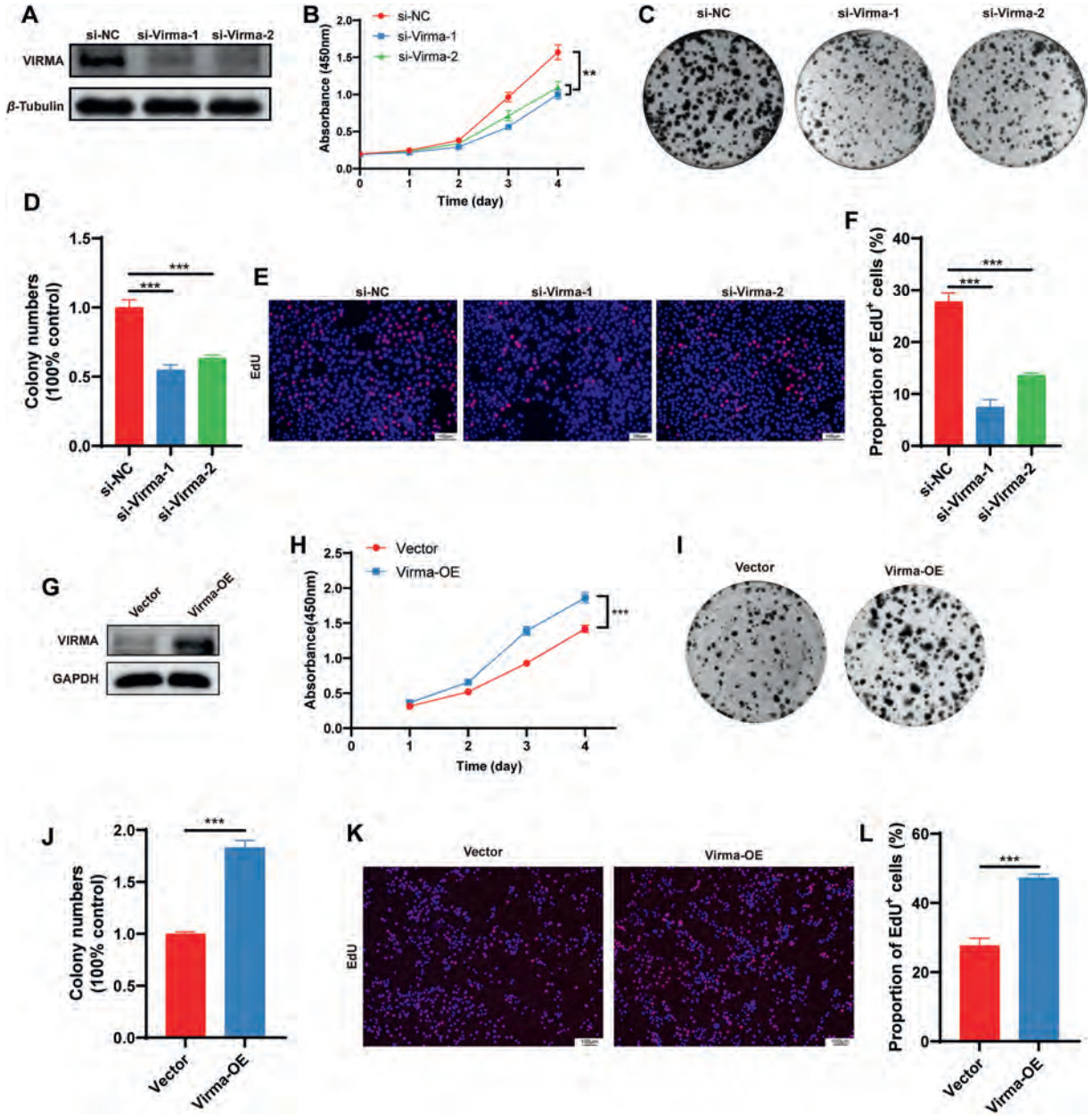

Figure 4 VIRMA promotes the proliferation of AML12 cells. (A−F) The effects of *Virma* silencing in AML12 cells (A) on proliferation capacity using CCK8 assays (B), Colony formation assays (C, D), EdU labeling assays and their (E, F) quantitative statistical analysis, respectively (scale bar = 50 μm). (G−L) The effects of VIRMA overexpression in AML12 cells (G) on proliferation capacity using CCK8 assays (H), Colony formation assays (I, J), EdU labeling assays and their (K, L) quantitative statistical analysis, respectively (scale bar = 100 μm). Data are presented as mean ± SEM ($n = 5$), $^{*}P < 0.05$; $^{**}P < 0.01$; $^{***}P < 0.001$; ns, $P > 0.05$.

in vitro promoted the expression of SHQ1 (Fig. 6H). Subsequently, we evaluated whether the biological effects of VIRMA depend on SHQ1. CCK-8 assays, colony formation experiments, and EdU labeling assays suggested that the knockdown of *Shq1* reversed the enhanced proliferation capacity of AML12 cells induced by *Virma* overexpression (Fig. 6I−M). Importantly, the increase in p-AKT^{Ser473}/t-AKT expression levels induced by *Virma* overexpression was also inhibited by the downregulation of SHQ1 (Fig. 6H). This observation suggests that VIRMA affects the proliferation capacity of AML12 by regulating SHQ1 expression, and this regulatory effect may be associated with the activation of the AKT signaling pathway.

Compared with the overexpression of wild-type *Shq1* (*Shq1*-WT), the mRNA (Fig. S5F) and protein levels of SHQ1(Fig. 7A)

48, and 72 h post CCl_4 treatment. G1 phase protein: CyclinD1; S phase proteins: CyclinA2 and CDK2; G2 phase proteins: CyclinB1 and CDK1. (F−H) Immunohistochemical staining for Ki67, BrdU, and p-H3S10 in liver tissues of two groups at indicated time points after CCl_4 induction, along with statistical analysis of the percentage of positively stained cells (scale bar = 100 μm). Data are presented as mean ± SEM ($n = 5$), $^{*}P < 0.05$; $^{**}P < 0.01$; $^{***}P < 0.001$; ns, $P > 0.05$.

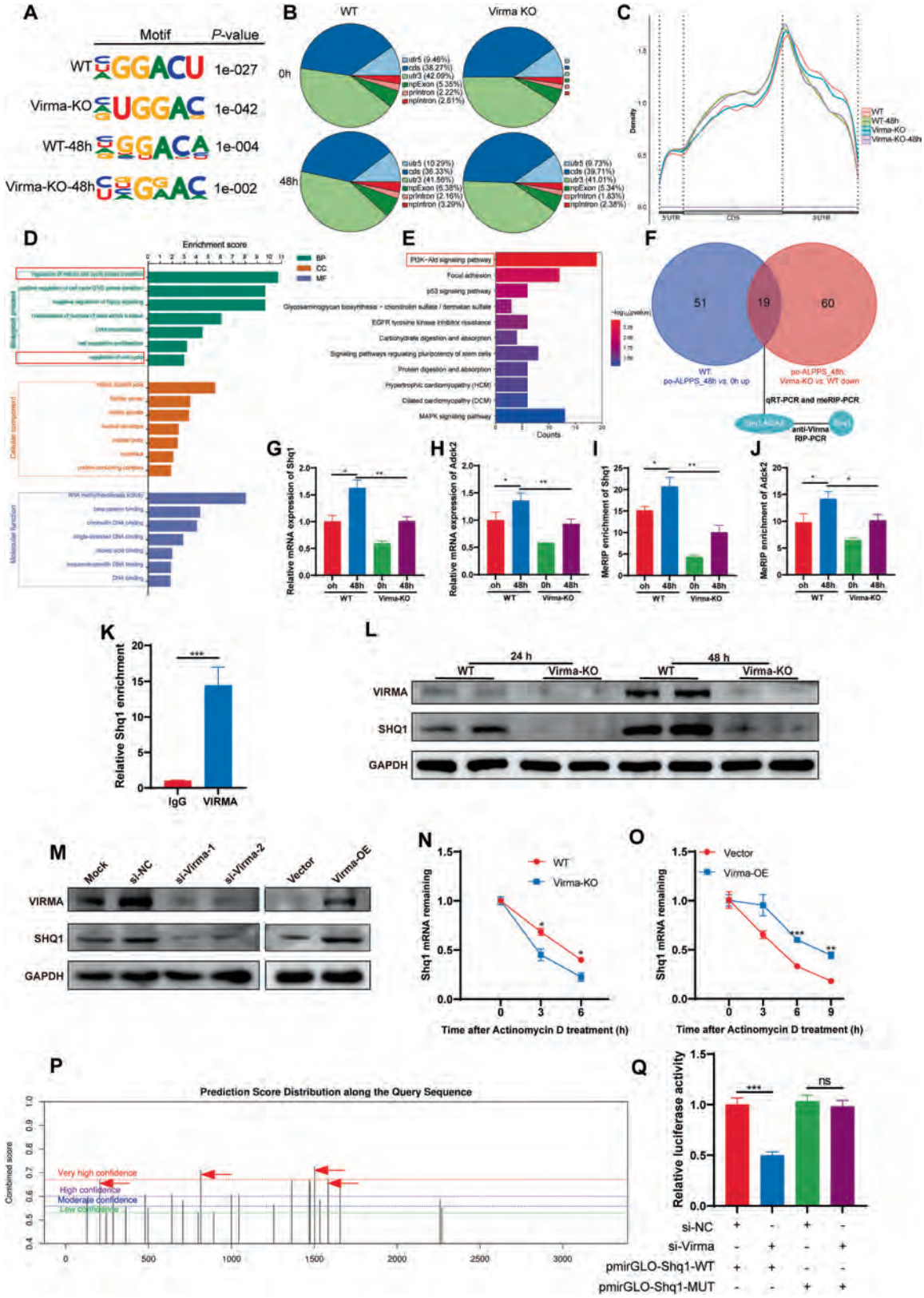

Figure 5 SHQ1 was identified as a downstream target of VIRMA-mediated m6A modification. (A–C) Specific motif sequences (A) and distribution of m6A peaks (B, C) of mice liver tissues from the four groups. (D, E) Gene Ontology analysis (D) and Kyoto Encyclopedia of Genes and Genomes pathway analysis (E) of the primary m6A-altered genes during liver regeneration in WT and *Virma*-KO mice after 48 h of ALPPS surgery. (F) The schematic strategy for identifying the candidate downstream targets of VIRMA during regeneration. A total of 19 genes met the requirements that their expression was up-regulated 48 h after ALPPS and subsequently decreased following *Virma* knockout. Using qRT-PCR and methylated RNA immunoprecipitation (meRIP)-PCR, we confirmed that 2 out of the 19 genes exhibited this expression pattern. Further

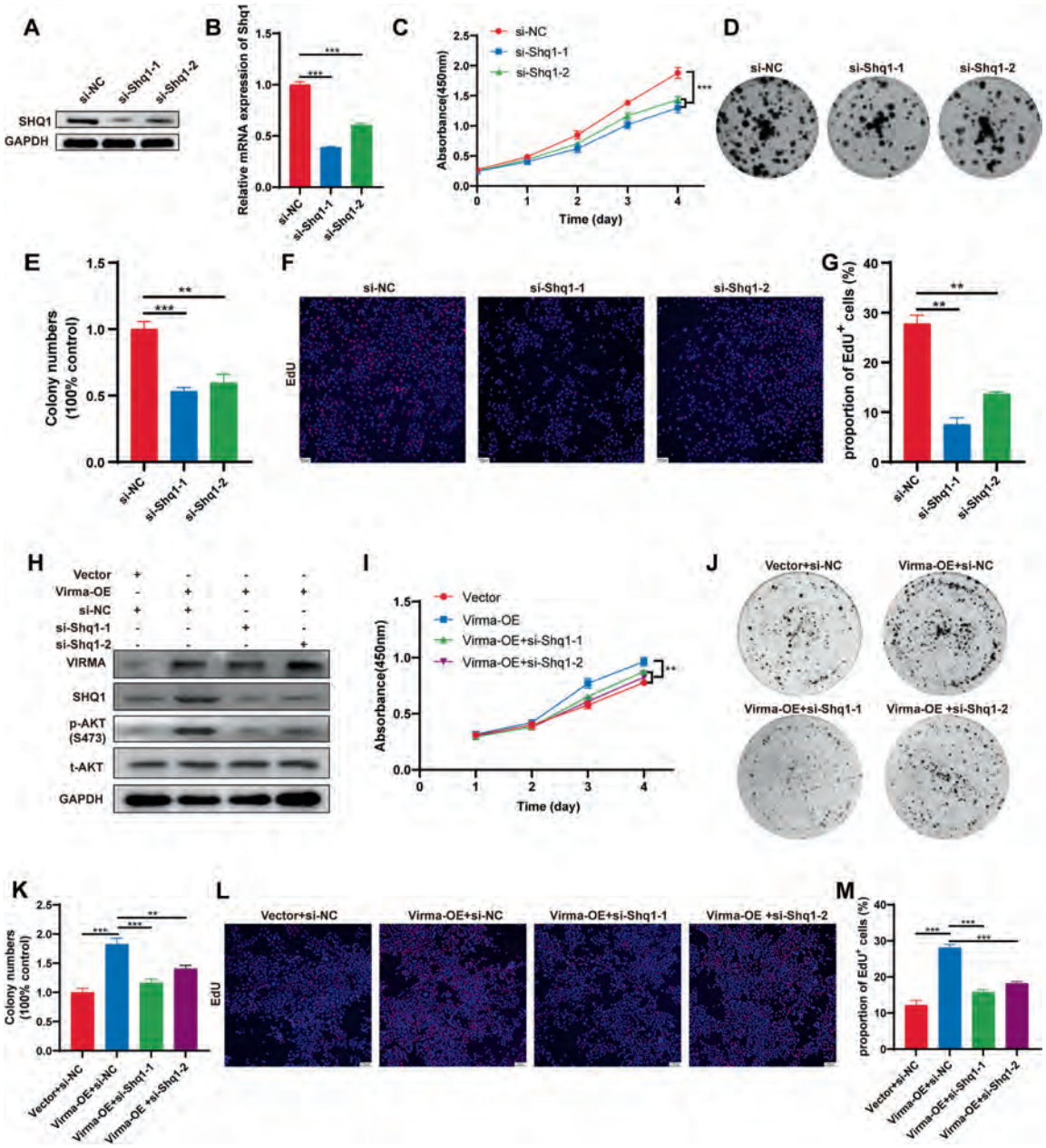

Figure 6 Knockdown of *Shq1* inhibits the proliferation capacity of AML12 cells. (A) Western blotting for SHQ1, p-AKT(Ser473), and t-AKT after silencing *Shq1* in AML12. (B−G) The effects of *Shq1* silencing in AML12 (B) on proliferation capacity using CCK8 assays (C), colony formation assays (D, E), EdU labeling assays and their (F, G) quantitative statistical analysis, respectively (Scale bar = 100 μm). (H) Western blotting for VIRMA, SHQ1, p-AKT(Ser473), and t-AKT after silencing *Shq1* in VIRMA-overexpressing AML12. (I−M) The effects of silencing *Shq1* in VIRMA-overexpressing AML12 on proliferation capacity using CCK8 assays (I), Colony formation assays (J, K), EdU labeling assays and their (L, M) quantitative statistical analysis, respectively, (Scale bar = 100 μm). Data are presented as mean ± SEM ($n = 5$), *$P < 0.05$; **$P < 0.01$; ***$P < 0.001$; ns, $P > 0.05$.

analysis using anti-VIRMA RNA immunoprecipitation (RIP)-PCR revealed that only *Shq1* among these 2 genes possessed the ability to directly bind with VIRMA. (G, H) qRT-PCR of liver tissues for *Shq1* and *Adck2*. (I, J) MeRIP-qPCR analysis of *Shq1* and *Adck2* mRNA in liver tissues. (K) RIP-qPCR analysis of the enrichment of *Shq1* mRNA on VIRMA relative to IgG in AML12 cells. (L) Western blotting for VIRMA and SHQ1 in liver tissues. (M) Western blotting for VIRMA and SHQ1 after silencing or overexpressing *Virma* in AML12 cells. (N, O) qRT-PCR analysis for the expression of *Shq1* mRNA in AML12 cells-overexpressing or knocking down *Virma* treated with Actinomycin D at indicated time points. (P) Prediction of m6A methylation sites of *Shq1* using the SRAMP database. (Q) Relative luciferase activity in NIH/3T3 cells co-transfected with luciferase reporter pmirGLO-*Shq1*-WT or pmirGLO-*Shq1*-MUT and VIRMA siRNAs or the control. Data are shown as the relative ratio of firefly luciferase activity to *Renilla* luciferase activity. Data are presented as mean ± SEM ($n = 5$), *$P < 0.05$; **$P < 0.01$; ***$P < 0.001$; ns, $P > 0.05$.

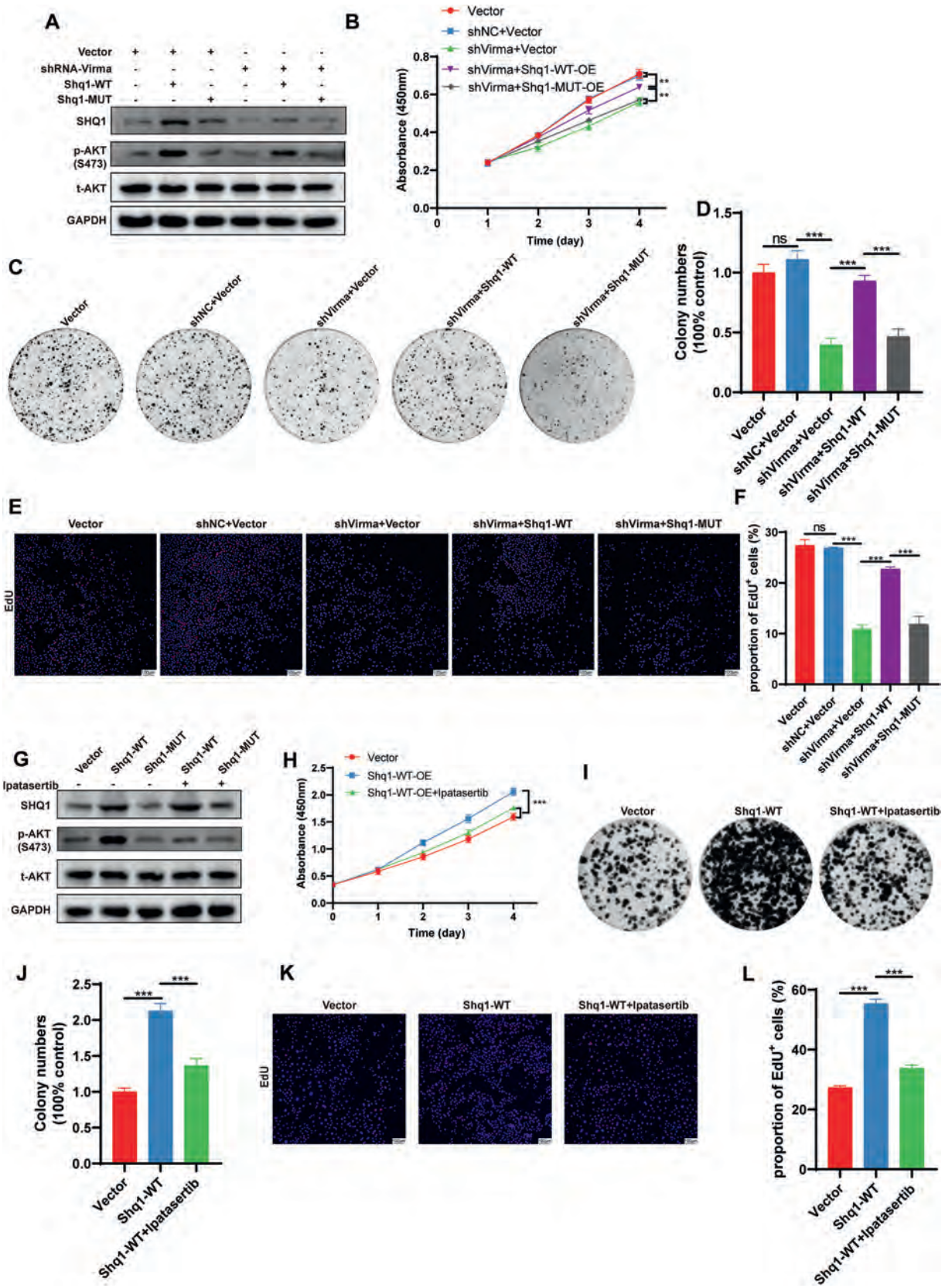

Figure 7 Overexpression of SHQ1 promotes AML12 cell proliferation. (A) Western blotting for p-AKT(Ser473) and t-AKT after overexpressing *Shq1*-WT or *Shq1*-MUT in *Virma*-silenced AML12 cells. (B−F) After overexpressing *Shq1*-WT or *Shq1*-MUT in *Virma*-silenced AML12 cells, cell proliferation capacity was determined using CCK8 assays (B), Colony formation assays (C, D), EdU labeling assays and their (E, F) quantitative statistical analysis, respectively (scale bar = 100 μm). (G) Western blotting for SHQ1, p-AKT(Ser473), and t-AKT after

were significantly reduced in the *Shq1*-MUT (m^6A site mutant) overexpression group. Additionally, knocking down *Virma* inhibited the expression of p-AKT^{Ser473}/t-AKT, while overexpression of WT *Shq1* reversed the inhibitory effect of *Virma* knockdown on p-AKT^{Ser473}/t-AKT expression (Fig. 7A). Notably, the ability of *Shq1*-MUT to counteract the *Virma* knockdown-induced decrease in p-AKT/t-AKT expression was significantly lower than that of WT *Shq1* overexpression (Fig. 7A). Furthermore, reintroducing WT *Shq1* markedly rescued the inhibitory effect of *Virma* knockdown on cell proliferation, whereas overexpression of *Shq1*-MUT failed to exert a comparable effect, as demonstrated by CCK-8 assays, colony formation experiments, and EdU labeling assays (Fig. 7B−F). These results indicate that m6A modification sites of *Shq1* are crucial for its function in VIRMA-mediated hepatocyte proliferation, and p-AKT^{Ser473}/t-AKT is involved in this process. As mentioned earlier, pathway analysis revealed that the loss of VIRMA enriched the PI3K/AKT signaling pathway, also, previous studies have reported that loss of the FOXP1−SHQ1 complex can lead to decreased phosphorylation levels of AKT at the Ser473 site in solid tumors[35]. Here we treated AML12 cells overexpressing SHQ1 with the AKT-specific inhibitor ipatasertib[36-38], which significantly reduced p-AKT^{Ser473}/t-AKT levels without affecting SHQ1 expression (Fig. 7G). Cellular functional experiments demonstrated that stable overexpression of SHQ1 significantly enhanced the proliferation capacity of AML12 cells, as evidenced by CCK-8 proliferation assays, colony formation assays, and EdU labeling assays results (Fig. 7H−L). Convincingly, treatment with ipatasertib significantly reversed the promoting effect of SHQ1 on the proliferation capacity of AML12 cells (Fig. 7H−L), suggesting that the enhancement of proliferation capacity by SHQ1 in AML12 cells depends, to some extent, on the activation status of AKT. To elucidate the regulatory mechanism by which SHQ1 influences hepatocyte proliferation, we performed immunoprecipitation combined with mass spectrometry analysis, successfully enriching a series of potential interacting proteins (Supporting Information Table S2). Interestingly, mass spectrometry results revealed that RICTOR, a key signaling molecule in the PI3K/AKT pathway, may interact with SHQ1 (Supporting Information Fig. S6A). As a crucial component of mTORC2, RICTOR primarily regulates the phosphorylation of AKT at Ser473, thereby enhancing AKT activity[39]. We further validated the interaction between SHQ1 and RICTOR through co-IP assays (Fig. S6B). Next, we investigated the role of RICTOR in the regulation of AKT^{Ser473} phosphorylation. Western blot analysis demonstrated that *Rictor* knockdown significantly reduced the expression of p-AKT^{Ser473}/t-AKT, whereas *Rictor* overexpression had the opposite effect (Fig. S6C). As expected, siRNA-mediated depletion of *Rictor* attenuated the promoting effect of *Shq1* overexpression on AKT^{Ser473} phosphorylation. Conversely, reintroducing *Rictor* restored the reduction in AKT^{Ser473} phosphorylation caused by *Shq1* knockdown (Fig. S6D and S6E). Functionally, colony formation and CCK-8 proliferation assays revealed that *Shq1* overexpression significantly enhanced hepatocyte proliferation. In contrast, *Rictor* depletion impaired this effect. Furthermore, reintroducing *Rictor* effectively rescued the decline in hepatocyte proliferation induced by *Shq1* knockdown (Fig. S6F−S6I).

Collectively, these findings suggest that SHQ1 plays a crucial role in VIRMA-mediated hepatocyte proliferation through its m6A modification sites. This process is driven by SHQ1's interaction with RICTOR, which promotes AKT^{Ser473} phosphorylation and activates the PI3K/AKT signaling pathway.

3.6. m6A-binding protein HNRNPA2B1 enhances the stability of Shq1 mRNA

The process of m6A methylation is primarily regulated by "writers" and "erasers" that control the methylation levels of RNA, while "readers" recognize methylated RNA molecules and participate in regulating various biological processes such as transcription, splicing, stability, and transportation of RNA. To understand which potential readers may be involved in this process, we assessed the mRNA expression levels of "readers" (*Ythdc1*, *Ythdc2*, *Ythdf1*, *Ythdf2*, *Ythdf3*, *Hnrnpa2b1*, *Igf2bp1*, *Igf2bp2*, *and Igf2bp3*) in ALPPS and CCl_4 models (Fig. 8A and B). The results revealed that *Ythdc2*, *Ythdf2*, *Ythdf3*, *Hnrnpa2b1*, and *Igf2bp2* exhibited an upward trend in both the CCl_4 and ALPPS models, with *Hnrnpa2b1* showing the greatest increase. Based on this finding, we further evaluated the potential role of HNRNPA2B1 in SHQ1, and found a significant decrease in the protein expression level of SHQ1 after silencing *Hnrnpa2b1* in AML12 cells (Fig. 8C). Then, we demonstrated the interaction between HNRNPA2B1 and *Shq1* (Fig. 8D), and revealed that silencing of *Hnrnpa2b1* could resulted in decreased stability of *Shq1* mRNA (Fig. 8E). On the other hand, results from dual-luciferase assays using constructed pmirGLO-*Shq1*-WT and pmirGLO-*Shq1*-MUT plasmids also showed that the luciferase activity of pmirGLO-*Shq1*-WT significantly decreased after silencing *Hnrnpa2b1*, while the activity of pmirGLO-*Shq1*-MUT did not change significantly after silencing *Hnrnpa2b1* (Fig. 8F), indicating that the regulation of *Shq1* expression by *Hnrnpa2b1* depends on m6A modification. To investigate the effect of m6A site modification on the mRNA stability of *Shq1*, we transfected AML12 cells with *Shq1*-CDS and *Shq1*-MUT plasmids and evaluated the *Shq1* mRNA stability under actinomycin D treatment. Compared with the Shq1-CDS transfection group, the *Shq1*-MUT transfection group exhibited a decreased stability of *Shq1* mRNA, indicating the important role of m6A sites in maintaining *Shq1* mRNA stability (Fig. 8G).

3.7. VIRMA promotes liver regeneration by enhancing SHQ1 expression

To confirm whether SHQ1 is the primary contributor to liver regeneration promoted by VIRMA *in vivo*, we assessed whether the introduction of SHQ1 could rescue the detrimental effects of *Virma* knockout on liver regeneration. We achieved liver-specific overexpression of *Shq1* in the *Virma*-KO mouse using adeno-associated virus 8 (AAV8) vectors (Fig. 9A). Over designated time points post-ALPPS surgery, we observed a significant reversal of reduced liver regeneration rate caused by *Virma* knockout in mice overexpressing *Shq1*, as measured by FLR/BW and liver regeneration rate (Fig. 9B and C). Additionally, serum markers of liver function, including ALT, AST, and TBIL, showed a significant reversal of the elevation induced by *Virma* knockout in mice overexpressing SHQ1 (Fig. 9D−F). Immunohistochemical analysis of liver regeneration markers Ki67, BrdU, and p-H3S10 at the 48-h post-ALPPS surgery revealed that the overexpression of SHQ1 effectively reversed the decrease of these markers caused by *Virma* knockout (Fig. 9G−I). Consistently, H&E staining further demonstrated that SHQ1 overexpression effectively restored mitotic activity (indicated by arrows), which was significantly reduced in *Virma*-KO mice (Fig. S5G). Overall, our study elucidates that during liver regeneration, VIRMA upregulates SHQ1 expression by promoting its m6A modification. In this mechanism, HNRNPA2B1, as a "reader" capable of recognizing

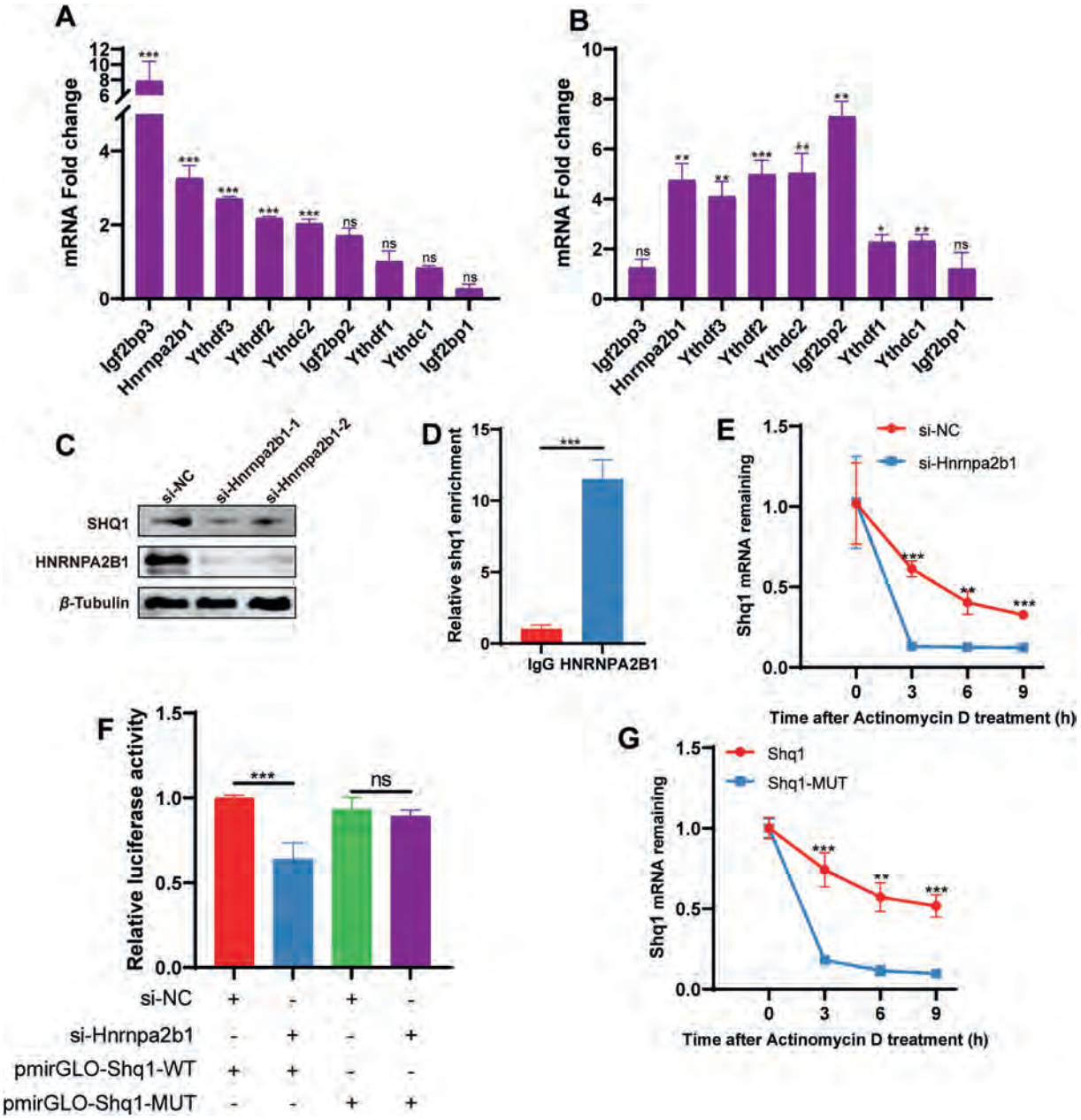

Figure 8 Knockdown of *Hnrnpa2b1* reduces *Shq1* mRNA stability. (A, B) qRT-PCR analysis of candidate m6A reader proteins in liver tissues from the Associating Liver Partition and Portal vein Ligation for Staged Hepatectomy (ALPPS) model (A) and carbon tetrachloride (CCl_4) model (B). (C) Western blotting for SHQ1 and HNRNPA2B1 after silencing *Hnrnpa2b1* in AML12. (D) RNA immunoprecipitation (RIP)-qPCR analysis of the enrichment of *Shq1* mRNA on HNRNPA2B1 relative to IgG in AML12 cells. (E) qRT-PCR analysis for the expression of *Shq1* mRNA in *Hnrnpa2b1*-silenced AML12 cells treated with Actinomycin D at indicated time points. (F) Relative luciferase activity in NIH/3T3 cells co-transfected with luciferase reporter pmirGLO-*Shq1*-WT or pmirGLO-*Shq1*-MUT and *Hnrnpa2b1* siRNAs or the control. Data are shown as the relative ratio of firefly luciferase activity to renilla luciferase activity. (G) qRT-PCR analysis for the expression of *Shq1* mRNA in AML12 cells overexpressing *Shq1*-WT or *Shq1*-MUT treated with Actinomycin D at indicated time points. Data are presented as mean ± SEM ($n = 5$), $^{*}P < 0.05$; $^{**}P < 0.01$; $^{***}P < 0.001$; ns, $P > 0.05$.

treating with ipatasertib for 24 h in *Shq1*-WT or *Shq1*-MUT overexpressing AML12 cells. (H−L) After treating with ipatasertib for 24 h in *Shq1*-WT overexpressing AML12 cells, cell proliferation capacity was determined using CCK8 assays (H), Colony formation assays (I, J), EdU labeling assays (K, L) and their quantitative statistical analysis, respectively (scale bar = 100 μm). Data are presented as mean ± SEM ($n = 5$), $^{*}P < 0.05$; $^{**}P < 0.01$; $^{***}P < 0.001$; ns, $P > 0.05$.

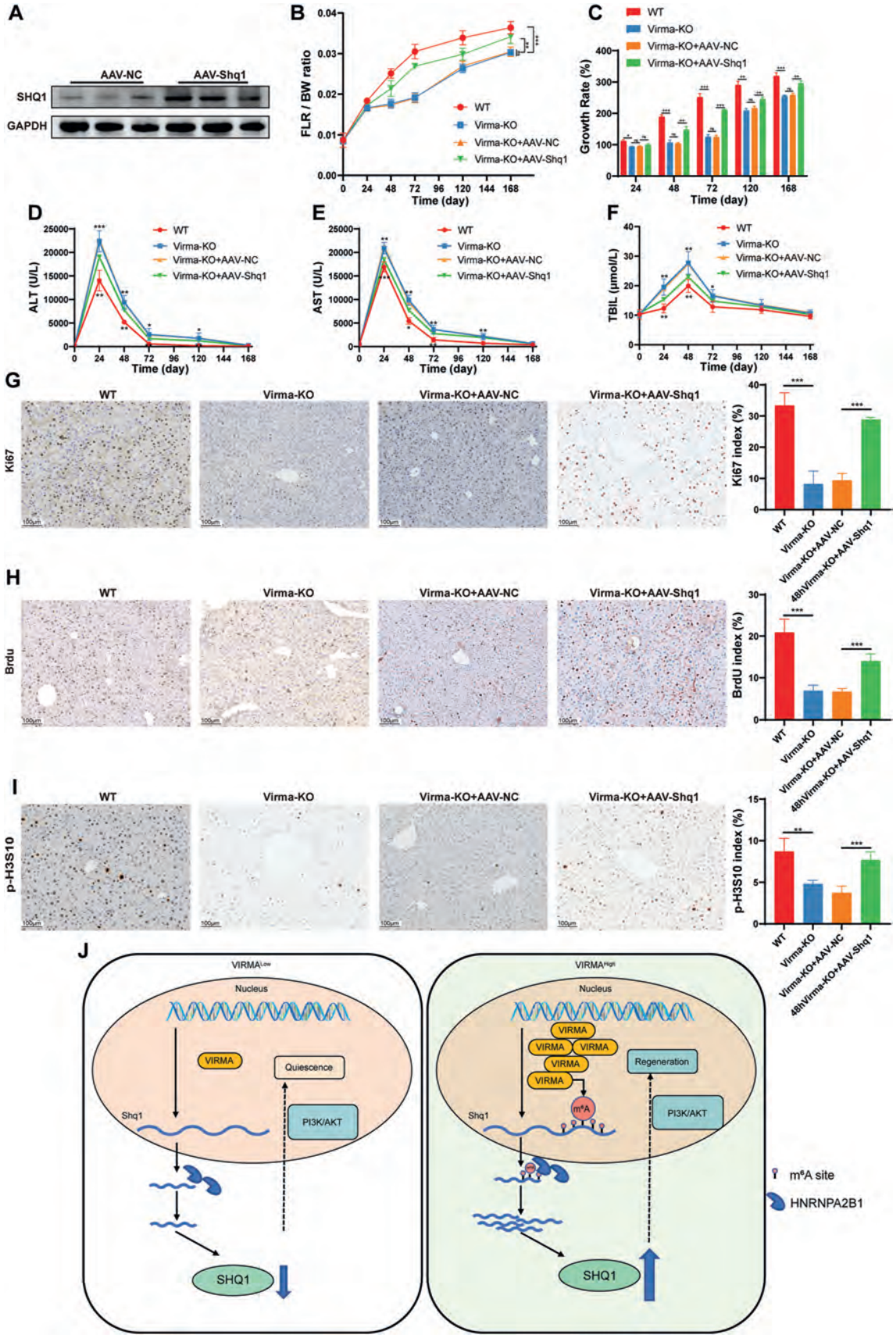

Figure 9 VIRMA promotes liver regeneration by enhancing SHQ1 expression. (A) Effects of SHQ1 overexpression in mice *via* tail vein injection. (B) FLR/BW of mice at designated time points after ALPPS surgery. (C) Liver regeneration rate of mice at designated time points after

and binding to m6A-modified *Shq1* mRNA, further enhances the stability of *Shq1* mRNA, leading to increased SHQ1 protein expression levels. Overall, our findings indicate that the upregulation of SHQ1 expression activates the PI3K/AKT signaling pathway, which is crucial for promoting liver regeneration (Fig. 9J).

4. Discussion

Liver regeneration is a complex process, and the proliferation of residual hepatocytes following liver injury is a crucial step in liver regeneration. After stimulation, various pro-regenerative molecules and signaling pathways are activated in this process[40-43]. In this study, both *in vitro* and *in vivo* experiments demonstrated the significant role of VIRMA in regulating mouse hepatocyte proliferation and liver regeneration. We found that VIRMA is upregulated in the early stages after ALPPS surgery in mice, and the global m6A modification level in the liver is significantly increased during this stage. Liver-specific knockout of *Virma* impairs liver regeneration capacity. Mechanistically, the loss of VIRMA leads to a reduction in m6A modification of its downstream direct target, SHQ1. The decreased binding capacity of SHQ1 with the "reader" HNRNPA2B1 results in decreased expression of SHQ1, thereby impairing hepatocyte proliferation and liver regeneration.

Multiple studies have demonstrated the crucial involvement of epigenetic modifications in liver regeneration[44-47]. As a prevalent form of epigenetic modification, m6A methylation modification is the most common modification in eukaryotic RNA[48]. m6A modification is dynamic and reversible, with regulatory factors typically including three types: "writers", "erasers", and "readers". Writers are responsible for methylation modification, erasers remove methylation modifications[49]. Writers typically include Mettl3/Mettl14, VIRMA, WTAP, ZC3H13, and RBM15/RBM15B. VIRMA primarily guides methyltransferase components to specific RNA regions to assist in catalyzing m6A modification[7], and its modification efficiency exceeds that of Mettl3/Mettl14[15]. As research on m6A progresses, its role in liver regeneration is gradually being recognized. One study indicated that mutations in Mettl14 could suppress liver regeneration by inhibiting certain hepatocyte growth factors[13]. Another study suggested that the loss of Mettl14, rather than Mettl3, leads to decreased m6A modification levels in multiple mRNA transcripts, triggering endoplasmic reticulum stress and inhibiting liver regeneration[14]. m6A modification levels are upregulated in the early stages of liver regeneration, during which a large number of genes are activated to promote liver regeneration[14]. Our data indicate that VIRMA, as a core component of the m6A methyltransferase complex, is also dramatically upregulated during this stage. We observed lower levels of total m6A modification in liver-specific *Virma* knockout mice after ALPPS surgery, confirming the significant role of VIRMA in m6A modification.

We generated liver-specific *Virma* knockout mice, and although *Virma* deletion did not show significant effects on liver homeostasis in quiescent mice, it severely impaired liver regeneration after ALPPS surgery and CCl_4 induction. Previous studies have shown that the accumulation of monocyte-derived macrophages is crucial for the repair of necrotic liver regions[50]. In our CCl_4 model, the delayed tissue repair observed in the *Virma*-KO group may be associated with a reduced infiltration of monocyte-derived macrophages. To explore its potential mechanism of action, we employed MeRIP-seq to analyze the m6A modification changes induced by VIRMA deficiency and the corresponding transcripts. Through validation, we identified SHQ1 as an important downstream target of VIRMA during liver regeneration. *Virma* knockout reduced the m6A modification level of *Shq1*, leading to decreased expression of *Shq1*. We also found that *Shq1* and *Adck2* exhibited a significant increase in m6A modification after ALPPS. Notably, even in *Virma*-KO mice, hepatic m6A levels still showed a partial increase post-ALPPS, suggesting that *Virma* upregulation is not the sole contributor to this elevation. Instead, this increase may be closely linked to other components of the m6A methyltransferase complex, such as METTL3 and METTL14. It has been reported that m6A modification further affects mRNA stability and subsequent translation processes by altering RNA structural domains or influencing the specificity recognition process of readers[51]. RNA-binding protein HNRNPA2B1 has recently been identified as a reader protein involved in m6A modification[52]. By recognizing and binding to m6A-modified RNA, HNRNPA2B1 influences the fate of these RNAs, including their processing, localization, and translation, thereby regulating cellular responses and physiological processes. One study found that it promotes cell proliferation and disease progression by recognizing the m6A site of ILF3 and enhancing the stability of ILF3 mRNA transcripts[53]. In this study, we found that VIRMA promotes the expression of SHQ1 in an m6A-HNRNPA2B1-dependent manner.

SHQ1 is commonly involved in the maturation of H/ACA small nuclear RNAs, which typically participate in RNA splicing[54]. By assisting in the assembly of small nucleolar ribonucleoproteins, SHQ1 indirectly promotes the biogenesis of functional ribosomes necessary for protein synthesis to maintain genomic stability[55]. Despite extensive studies on the biochemical role and mechanism of SHQ1 in H/ACA snoRNP assembly, its biological functions in mammalian cells, particularly hepatocytes, remain relatively unknown. Recent studies have demonstrated that *Shq1* depletion significantly inhibits the growth of T-acute lymphoblastic leukemia cell[55]. Here, we provide the first evidence that the lack of SHQ1 inhibits the proliferation of hepatocyte. Furthermore, we observed that overexpression of WT *Shq1*, but not *Shq1*-MUT, reverses the cell proliferation inhibition caused by VIRMA deletion.

Activation of the PI3K/AKT pathway promotes various functions, including cell growth, proliferation, and progression

Associating Liver Partition and Portal vein Ligation for Staged Hepatectomy (ALPPS) surgery, calculated by the formula (postoperative FLR/BW−initial FLR/BW)/(initial FLR/BW). (D−F) Serum levels of ALT, AST, and TBIL in mice at designated time points after ALPPS surgery. (G−I) Immunohistochemical staining results for Ki67, BrdU, and p-H3S10 in liver tissue of mice at designated time points after ALPPS surgery, along with statistical analysis of the percentage of positive stained cells (scale bar = 100 μm). (J) A proposed model illustrating promoted effects of VIRMA on liver regeneration. VIRMA enhances liver regeneration by stabilizing m6A-modified *SHQ1* mRNA *via* HNRNPA2B1 binding, thereby activating the PI3K/AKT pathway and promoting hepatocyte proliferation. Data are presented as mean ± SEM ($n = 5$), $^{*}P < 0.05$; $^{**}P < 0.01$; $^{***}P < 0.001$; ns, $P > 0.05$.

through the cell cycle. Phosphorylation of AKT is a key event in the activation of this pathway and is essential for regulating cellular functions[56,57]. Following liver injury or hepatectomy, AKT is activated and phosphorylated, thereby triggering downstream signaling pathways necessary for liver regeneration and repair. Inhibition of this pathway significantly abolishes normal liver regenerative responses[58]. The increase in the pAKT/AKT ratio is fundamental for the restoration of glucose-dependent liver metabolic processes during liver regeneration[59]. Previous studies have indicated that loss of FOXP1-SHQ1 leads to decreased phosphorylation levels at the Ser473 site of AKT in solid tumors[35]. In this study, we observed that SHQ1-mediated activation of the PI3K/AKT pathway promotes the proliferation of hepatocyte, while treatment with the AKT-specific inhibitor ipatasertib significantly suppresses hepatocyte proliferation.

5. Conclusions

Our data demonstrate a close association between m6A modification and compensatory liver regeneration following ALPPS surgery and acute injury. During the early stages of liver regeneration, increased expression of VIRMA in the liver correlates with increased hepatocyte proliferation and accelerated cell cycle progression. Our study unveils a novel mechanism whereby loss of VIRMA leads to decreased m6A modification of *Shq1* mRNA. Reduced binding capacity of the m6A-binding protein HNRNPA2B1 to SHQ1 results in decreased mRNA stability and subsequent downregulation of SHQ1 expression. Furthermore, downregulation of SHQ1 inhibits the PI3K/AKT pathway, thereby suppressing hepatocyte proliferation and ultimately hindering liver regeneration.

Acknowledgments

This work was supported by grants from the National multidisciplinary collaborative diagnosis and treatment capacity building project for major diseases (TJZ202104, China), the Natural Science Foundation of China (82270643, 82070644, 82170621 and 82370645), the Science and Technology Major Program of Sichuan Province (2022ZDZX0019, China), 1.3.5 project for disciplines of excellence, West China Hospital, Sichuan University, China (ZYJC18008, ZYGD22006), Luzhou Municipal People's Government−Southwest Medical University Science and Technology Strategic Cooperation Project, China (2024LZXNYDJ045) and the Medical Science and Technology Development Project of Southwest Medical University, China (24297).

The authors are most grateful for Core Facility of West China Hospital for their technique support.

Author contributions

Hao Chen: Writing − original draft. Haichuan Wang: Conceptualization. Jiwei Huang: Writing − review & editing. Guoteng Qiu: Resources. Zheng Zhang: Software. Lin Xu: Data curation. Xiao Ma: Formal analysis. Zhen Wang: Supervision. Xiangzheng Chen: Methodology. Yong Zeng: Conceptualization.

Conflicts of interest

The authors declare no conflicts of interest that pertain to this work.

Appendix A. Supporting information

Supporting information to this article can be found online at https://doi.org/10.1016/j.apsb.2025.07.025.

References

1. Huppert SS, Schwartz RE. Multiple facets of cellular homeostasis and regeneration of the mammalian liver. *Annu Rev Physiol* 2023;**85**:469−93.
2. Fan S, Gao Y, Zhao P, Xie G, Zhou Y, Yang X, et al. Fenofibrate-promoted hepatomegaly and liver regeneration are PPARalpha-dependent and partially related to the YAP pathway. *Acta Pharm Sin B* 2024;**14**:2992−3008.
3. Mitchell C, Willenbring H. A reproducible and well-tolerated method for 2/3 partial hepatectomy in mice. *Nat Protoc* 2008;**3**:1167−70.
4. Fausto N, Campbell JS, Riehle KJ. Liver regeneration. *Hepatology* 2006;**43**:S45−53.
5. Wang B, Shen H, Wei Y, Liu F, Yang Y, Yu H, et al. Balance of Gata3 and Ramp2 in hepatocytes regulates hepatic vascular reconstitution in postoperative liver regeneration. *J Hepatol* 2024;**80**:309−21.
6. Robles-Campos R, Brusadin R, Lopez-Lopez V, Lopez-Conesa A, Navarro-Barrios A, Gomez-Valles P, et al. A new surgical technique variant of partial ALPPS (Tourniquet Partial-ALPPS). *Ann Surg* 2021;**273**:e22−4.
7. Jiang X, Liu B, Nie Z, Duan L, Xiong Q, Jin Z, et al. The role of m6A modification in the biological functions and diseases. *Signal Transduct Targeted Ther* 2021;**6**:74.
8. Fu Y, Dominissini D, Rechavi G, He C. Gene expression regulation mediated through reversible m^6A RNA methylation. *Nat Rev Genet* 2014;**15**:293−306.
9. Zhang H, Lu L, Yi C, Jiang T, Lu Y, Yang X, et al. BRD4 regulates m^6A of *ESPL1* mRNA *via* interaction with ALKBH5 to modulate breast cancer progression. *Acta Pharm Sin B* 2025;**15**:1552−70.
10. Meyer KD, Jaffrey SR. Rethinking m^6A readers, writers, and erasers. *Annu Rev Cell Dev Biol* 2017;**33**:319−42.
11. Geula S, Moshitch-Moshkovitz S, Dominissini D, Mansour AA, Kol N, Salmon-Divon M, et al. Stem cells. m6A mRNA methylation facilitates resolution of naive pluripotency toward differentiation. *Science* 2015;**347**:1002−6.
12. Wu Z, Shi Y, Lu M, Song M, Yu Z, Wang J, et al. METTL3 counteracts premature aging *via* m6A-dependent stabilization of *MIS12* mRNA. *Nucleic Acids Res* 2020;**48**:11083−96.
13. Yang I, Oh SY, Jang S, Kim IY, Sung YM, Seong JK. Mettl14 mutation restrains liver regeneration by attenuating mitogens derived from non-parenchymal liver cells. *BMB Rep* 2022;**55**:633−8.
14. Cao X, Shu Y, Chen Y, Xu Q, Guo G, Wu Z, et al. Mettl14-mediated m^6A modification facilitates liver regeneration by maintaining endoplasmic reticulum homeostasis. *Cell Mol Gastroenterol Hepatol* 2021;**12**:633−51.
15. Schwartz S, Mumbach MR, Jovanovic M, Wang T, Maciag K, Bushkin GG, et al. Perturbation of m6A writers reveals two distinct classes of mRNA methylation at internal and 5′ sites. *Cell Rep* 2014;**8**:284−96.
16. Li N, Zhu Z, Deng Y, Tang R, Hui H, Kang Y, et al. KIAA1429/-VIRMA promotes breast cancer progression by m^6A-dependent cytosolic HAS2 stabilization. *EMBO Rep* 2023;**24**:e55506.
17. Zheng ZQ, Huang ZH, Liang YL, Zheng WH, Xu C, Li ZX, et al. VIRMA promotes nasopharyngeal carcinoma, tumorigenesis, and

metastasis by upregulation of E2F7 in an m6A-dependent manner. *J Biol Chem* 2023;**299**:104677.
18. Wang H, Chen W, Cui Y, Gong H, Li H. KIAA1429 protects hepatocellular carcinoma cells from ferroptotic cell death with a m^6A-dependent posttranscriptional modification of SLC7A11. *J Cell Mol Med* 2023;**27**:4118−32.
19. Zhou S, Yang K, Chen S, Lian G, Huang Y, Yao H, et al. CCL3 secreted by hepatocytes promotes the metastasis of intrahepatic cholangiocarcinoma by VIRMA-mediated *N*6-methyladenosine (m^6A) modification. *J Transl Med* 2023;**21**:43.
20. Grozdanov PN, Roy S, Kittur N, Meier UT. SHQ1 is required prior to NAF1 for assembly of H/ACA small nucleolar and telomerase RNPs. *RNA* 2009;**15**:1188−97.
21. Su H, Hu J, Huang L, Yang Y, Thenoz M, Kuchmiy A, et al. SHQ1 regulation of RNA splicing is required for T-lymphoblastic leukemia cell survival. *Nat Commun* 2018;**9**:4281.
22. Schlegel A, Lesurtel M, Melloul E, Limani P, Tschuor C, Graf R, et al. ALPPS: from human to mice highlighting accelerated and novel mechanisms of liver regeneration. *Ann Surg* 2014;**260**:839−46. ; discussion 46-7.
23. Du J, Liao W, Wang H, Hou G, Liao M, Xu L, et al. MDIG-mediated H3K9me3 demethylation upregulates Myc by activating OTX2 and facilitates liver regeneration. *Signal Transduct Targeted Ther* 2023;**8**: 351.
24. Finn RS, Zhu AX, Farah W, Almasri J, Zaiem F, Prokop LJ, et al. Therapies for advanced stage hepatocellular carcinoma with macrovascular invasion or metastatic disease: a systematic review and meta-analysis. *Hepatology* 2018;**67**:422−35.
25. Meng J, Zhao Z, Xi Z, Xia Q. Liver-specific Mettl3 ablation delays liver regeneration in mice. *Genes Dis* 2022;**9**:697−704.
26. Xia J, Zhou Y, Ji H, Wang Y, Wu Q, Bao J, et al. Loss of histone deacetylases 1 and 2 in hepatocytes impairs murine liver regeneration through Ki67 depletion. *Hepatology* 2013;**58**:2089−98.
27. Li Y, Kao GD, Garcia BA, Shabanowitz J, Hunt DF, Qin J, et al. A novel histone deacetylase pathway regulates mitosis by modulating Aurora B kinase activity. *Genes Dev* 2006;**20**:2566−79.
28. Dominissini D, Moshitch-Moshkovitz S, Schwartz S, Salmon-Divon M, Ungar L, Osenberg S, et al. Topology of the human and mouse m6A RNA methylomes revealed by m6A-seq. *Nature* 2012; **485**:201−6.
29. Haga S, Ogawa W, Inoue H, Terui K, Ogino T, Igarashi R, et al. Compensatory recovery of liver mass by Akt-mediated hepatocellular hypertrophy in liver-specific STAT3-deficient mice. *J Hepatol* 2005; **43**:799−807.
30. Pauta M, Rotllan N, Fernandez-Hernando A, Langhi C, Ribera J, Lu M, et al. Akt-mediated foxo1 inhibition is required for liver regeneration. *Hepatology* 2016;**63**:1660−74.
31. Alidou-D'Anjou I, Patel A, Sleiman S, Dragon F. Human SHQ1 variants R335C and A426V lead to severe ribosome biogenesis defects when expressed in yeast. *Front Genet* 2023;**14**:1240416.
32. Yue Y, Liu J, Cui X, Cao J, Luo G, Zhang Z, et al. VIRMA mediates preferential m^6A mRNA methylation in 3′UTR and near stop codon and associates with alternative polyadenylation. *Cell Discov* 2018;**4**: 10.
33. Ratnadiwakara M, Archer SK, Dent CI, Ruiz De Los Mozos I, Beilharz TH, Knaupp AS, et al. SRSF3 promotes pluripotency through Nanog mRNA export and coordination of the pluripotency gene expression program. *eLife* 2018;**7**:e37419.
34. Lan T, Li H, Zhang D, Xu L, Liu H, Hao X, et al. KIAA1429 contributes to liver cancer progression through *N*6-methyladenosine-dependent post-transcriptional modification of GATA3. *Mol Cancer* 2019;**18**:186.
35. Hieronymus H, Iaquinta PJ, Wongvipat J, Gopalan A, Murali R, Mao N, et al. Deletion of 3p13-14 locus spanning FOXP1 to SHQ1 cooperates with PTEN loss in prostate oncogenesis. *Nat Commun* 2017;**8**:1081.
36. Saura C, Roda D, Rosello S, Oliveira M, Macarulla T, Perez-Fidalgo JA, et al. A first-in-human phase I study of the ATP-competitive AKT inhibitor ipatasertib demonstrates robust and safe targeting of AKT in patients with solid tumors. *Cancer Discov* 2017;**7**: 102−13.
37. Hong Z, Zhang W, Ding D, Huang Z, Yan Y, Cao W, et al. DNA damage promotes TMPRSS2-ERG oncoprotein destruction and prostate cancer suppression *via* signaling converged by GSK3beta and WEE1. *Mol Cell* 2020;**79**:1008.
38. Salvadori G, Zanardi F, Iannelli F, Lobefaro R, Vernieri C, Longo VD. Fasting-mimicking diet blocks triple-negative breast cancer and cancer stem cell escape. *Cell Metab* 2021;**33**:2247.
39. Sarbassov DD, Guertin DA, Ali SM, Sabatini DM. Phosphorylation and regulation of Akt/PKB by the rictor−mTOR complex. *Science* 2005;**307**:1098−101.
40. Campana L, Esser H, Huch M, Forbes S. Liver regeneration and inflammation: from fundamental science to clinical applications. *Nat Rev Mol Cell Biol* 2021;**22**:608−24.
41. Michalopoulos GK, Bhushan B. Liver regeneration: biological and pathological mechanisms and implications. *Nat Rev Gastroenterol Hepatol* 2021;**18**:40−55.
42. Murata H, Yagi T, Iwagaki H, Ogino T, Sadamori H, Matsukawa H, et al. Mechanism of impaired regeneration of fatty liver in mouse partial hepatectomy model. *J Gastroenterol Hepatol* 2007;**22**: 2173−80.
43. Guo M, Jiang X, Ouyang H, Zhang X, Zhang S, Wang P, et al. Parabacteroides distasonis promotes liver regeneration by increasing beta-hydroxybutyric acid (BHB) production and BHB-driven STAT3 signals. *Acta Pharm Sin B* 2025;**15**:1430−46.
44. Wang S, Zhang C, Hasson D, Desai A, SenBanerjee S, Magnani E, et al. Epigenetic compensation promotes liver regeneration. *Dev Cell* 2019;**50**:43−56.e6.
45. Zhou Y, Zhang L, Ji H, Lu X, Xia J, Li L, et al. MiR-17−92 ablation impairs liver regeneration in an estrogen-dependent manner. *J Cell Mol Med* 2016;**20**:939−48.
46. Zhang C, Macchi F, Magnani E, Sadler KC. Chromatin states shaped by an epigenetic code confer regenerative potential to the mouse liver. *Nat Commun* 2021;**12**:4110.
47. Lee HJ, Hou Y, Chen Y, Dailey ZZ, Riddihough A, Jang HS, et al. Regenerating zebrafish fin epigenome is characterized by stable lineage-specific DNA methylation and dynamic chromatin accessibility. *Genome Biol* 2020;**21**:52.
48. Deng X, Qing Y, Horne D, Huang H, Chen J. The roles and implications of RNA m^6A modification in cancer. *Nat Rev Clin Oncol* 2023; **20**:507−26.
49. Huang H, Weng H, Chen J. m^6A modification in coding and non-coding RNAs: roles and therapeutic implications in cancer. *Cancer Cell* 2020;**37**:270−88.
50. Feng D, Xiang X, Guan Y, Guillot A, Lu H, Chang C, et al. Monocyte-derived macrophages orchestrate multiple cell-type interactions to repair necrotic liver lesions in disease models. *J Clin Investig* 2023; **133**:e166954.
51. Zhang LS, Dai Q, He C. Base-resolution sequencing methods for whole-transcriptome quantification of mRNA modifications. *Acc Chem Res* 2024;**57**:47−58.
52. Liu R, Zhong Y, Chen R, Chu C, Liu G, Zhou Y, et al. m^6A reader hnRNPA2B1 drives multiple myeloma osteolytic bone disease. *Theranostics* 2022;**12**:7760−74.
53. Jiang F, Tang X, Tang C, Hua Z, Ke M, Wang C, et al. HNRNPA2B1 promotes multiple myeloma progression by increasing AKT3 expression *via* m6A-dependent stabilization of ILF3 mRNA. *J Hematol Oncol* 2021;**14**:54.
54. Walbott H, Machado-Pinilla R, Liger D, Blaud M, Rety S, Grozdanov PN, et al. The H/ACA RNP assembly factor SHQ1 functions as an RNA mimic. *Genes Dev* 2011;**25**:2398−408.
55. Webster SF, Ghalei H. Maturation of small nucleolar RNAs: from production to function. *RNA Biol* 2023;**20**:715−36.
56. Liu R, Chen Y, Liu G, Li C, Song Y, Cao Z, et al. PI3K/AKT pathway as a key link modulates the multidrug resistance of cancers. *Cell Death Dis* 2020;**11**:797.

57. Chang F, Lee JT, Navolanic PM, Steelman LS, Shelton JG, Blalock WL, et al. Involvement of PI3K/Akt pathway in cell cycle progression, apoptosis, and neoplastic transformation: a target for cancer chemotherapy. *Leukemia* 2003;**17**:590−603.
58. Jackson LN, Larson SD, Silva SR, Rychahou PG, Chen LA, Qiu S, et al. PI3K/Akt activation is critical for early hepatic regeneration after partial hepatectomy. *Am J Physiol Gastrointest Liver Physiol* 2008; **294**:G1401−10.
59. Rejano-Gordillo CM, Gonzalez-Rico FJ, Marin-Diaz B, Ordiales-Talavero A, Nacarino-Palma A, Roman AC, et al. Liver regeneration after partial hepatectomy is improved in the absence of aryl hydrocarbon receptor. *Sci Rep* 2022;**12**:15446.